Global Release of Translational Repression Across *Plasmodium's* Host-to-Vector Transmission Event

Kelly T. Rios[1,6], James P. McGee[1,6], Aswathy Sebastian[2], Robert L. Moritz[4], Marina Feric[1,7], Sabrina Absalon[3], Kristian E. Swearingen[4], and Scott E. Lindner[1,5,6,#]

1. Department of Biochemistry and Molecular Biology, Pennsylvania State University, University Park, PA 16802
2. Huck Institutes of the Life Sciences, Pennsylvania State University, University Park, PA, 16802
3. Department of Pharmacology and Toxicology, Indiana University School of Medicine, Indianapolis, IN 46202
4. Institute for Systems Biology, Seattle, WA 98109
5. Huck Center for Malaria Research, Pennsylvania State University, University Park, PA, 16802
6. Center for Eukaryotic Gene Regulation, Pennsylvania State University, University Park, PA, 16802

#: Corresponding Author:

Scott E. Lindner, Ph.D.

W230B Millennium Science Complex

University Park, PA 16802

P: +1.814.867.4062

E: Scott.Lindner@psu.edu

Author ORCIDs:

Kelly T. Rios: 0000-0001-6662-6426

James P. McGee: 0000-0003-0225-1172

Aswathy Sebastian: 0000-0003-4936-5564

Robert L. Moritz: 0000-0002-3216-9447

Marina Feric: 0000-0001-7531-9305

Sabrina Absalon: 0000-0003-2468-8156

Kristian Swearingen: 0000-0002-6756-4471

Scott Lindner: 0000-0003-1799-3726

Keywords: Translational Repression, Malaria Transmission, RNA-seq, DIA Proteomics, Proximity Proteomics

Abstract:

Malaria parasites must be able to respond quickly to changes in their environment, including during their transmission between mammalian hosts and mosquito vectors. Therefore, before transmission, female gametocytes proactively produce and translationally repress mRNAs that encode essential proteins that the zygote requires to establish a new infection. This essential regulatory control requires the orthologues of DDX6 (DOZI), LSM14a (CITH), and ALBA proteins to form a translationally repressive complex in female gametocytes that associates with many of the affected mRNAs. However, while the release of translational repression of individual mRNAs has been documented, the details of the global release of translational repression have not. Moreover, the changes in spatial arrangement and composition of the DOZI/CITH/ALBA complex that contribute to translational control are also not known.

Therefore, we have conducted the first quantitative, comparative transcriptomics and DIA-MS proteomics of *Plasmodium* parasites across the host-to-vector transmission event to document the global release of translational repression. Using female gametocytes and zygotes of *P. yoelii*, we found that nearly 200 transcripts are released for translation soon after fertilization, including those with essential functions for the zygote. However, we also observed that some transcripts remain repressed beyond this point. In addition, we have used TurboID-based proximity proteomics to interrogate the spatial and compositional changes in the DOZI/CITH/ALBA complex across this transmission event. Consistent with recent models of translational control, proteins that associate with either the 5’ or 3’ end of mRNAs are in close proximity to one another during translational repression in female gametocytes and then dissociate upon release of repression in zygotes. This observation is cross-validated for several protein colocalizations in female gametocytes via ultrastructure expansion microscopy and structured illumination microscopy. Moreover, DOZI exchanges its interaction from NOT1-G in female gametocytes to the canonical NOT1 in zygotes, providing a model for a trigger for the release of mRNAs from DOZI. Finally, unenriched phosphoproteomics revealed the modification of key translational control proteins in the zygote. Together, these data provide a model for the essential translational control mechanisms used by malaria parasites to promote their efficient transmission from their mammalian host to their mosquito vector.

51 **Introduction:**

52 Early embryonic development in higher eukaryotes depends on essential, maternally supplied products for early gene
53 expression until the zygote can carry out its own gene expression program. This process, called the maternal-to-zygotic
54 transition (MZT) (1-3), involves the proactive generation of transcripts in the oocyte ahead of fertilization that are stored
55 in cytosolic mRNPs and are translationally repressed/silenced until fertilization occurs (4). The translation of these
56 maternally provided transcripts is essential for early zygotic development and directly precedes zygotic genome
57 activation (ZGA) subsequent *de novo* transcription by the zygote (3, 5).

58 Malaria parasites (*Plasmodium* spp.) use an MZT-like process to proactively transcribe, preserve, and translationally
59 repress mRNAs in female gametocytes until host-to-vector transmission occurs (6-9). For this essential regulatory
60 process, *Plasmodium* uses evolutionarily conserved RNA-binding protein regulators of translational repression, such as
61 the orthologues of DDX6 (DOZI), LSM14 / CAR-I / Trailer Hitch (CITH), ALBA family proteins, and others (7, 10). Evidence
62 for translational repression in female gametocytes in multiple *Plasmodium* species has come from gene-specific studies
63 as well as comparative transcriptomic and proteomic studies, which noted strong disparities in the abundances of
64 mRNAs and their corresponding proteins (6-14). One of the most rigorous studies, conducted by Lasonder and
65 colleagues, presented evidence for approximately 500 putatively translationally repressed transcripts in *P. falciparum*
66 female gametocytes (6). Based on these observations, the essential use of translational repression during parasite
67 transmission is predicted to provide a rapid means to produce the proteins needed to adapt to the new host
68 environment and overcome its physical barriers and immunological defenses. However, this model has not been
69 validated at a global level for the host-to-vector transmission event, such as by examining the extent of the release of
70 translational repression after fertilization and determining what proteins are made at very early time points.

71 While total comparative analyses of transcriptomic and proteomic expression of male and female gametocytes have
72 been published in recent years, the same comparative data are lacking for zygotes (6, 12, 14). Two recent publications
73 describe transcriptomic analyses of *Plasmodium* zygotes: a bulk RNA-seq study of *in vitro* cultured *P. berghei* zygotes,
74 and a single-cell RNA-seq study of the early *P. falciparum* mosquito stages isolated from the mosquito blood bolus
75 throughout the first twenty hours of infection (11, 15). These publications contribute significantly to our understanding
76 of transcription and gene regulation by specific ApiAP2 transcription factors in this stage and highlight the control of
77 gene expression early in mosquito stage establishment. Still, neither included a proteomic comparison to identify the
78 proteins expressed in this stage (11, 15). To date, the only published work to define the *Plasmodium* zygote proteome
79 was completed 15 years ago, from *in vitro* cultured zygotes from the avian malaria parasite *P. gallinaceum*, which was
80 completed prior to the release of its genomic sequence (16). The best evidence for the release of translational
81 repression in early mosquito-stage parasites is from single-gene studies that demonstrated that ookinete surface-
82 expressed and secreted proteins, as well as ApiAP2 transcription factors, are critical for parasite survival and

83 transmission (9, 11, 13, 17, 18). This key knowledge gap in our understanding of this essential host-to-vector
84 transmission strategy could therefore be resolved with a paired transcriptome and proteome of female gametocyte and
85 zygote stage parasites.

86 Translational repression in *Plasmodium* transmission stages is known to be mediated by RNA-binding proteins (reviewed
87 in (19)). In female gametocytes, members of the RNA-binding protein DOZI/CITH/ALBA complex contribute to preserving
88 and stabilizing specific transcripts (7, 10, 20, 21). When DOZI or CITH are absent, proper development of the zygote
89 cannot occur. Hundreds of transcripts were identified as interactors of PbDOZI in an RNA-immunoprecipitation
90 microarray study, and a large proportion of these bound transcripts overlap with those transcripts that decrease in
91 abundance when *pbdozi* was deleted, indicating their abundance may be directly or indirectly dependent on the
92 presence of DOZI (21). However, nothing is known about how the DOZI/CITH/ALBA (DCA) complex selects specific
93 mRNAs in female gametocytes or releases them for translation in zygotes.

94 To address these key knowledge gaps, here we have used quantitative, comparative transcriptomic and proteomic
95 approaches to identify translationally repressed transcripts in *P. yoelii* female gametocytes, which are then released for
96 translation following fertilization in early zygotes. Several of these proteins are essential to establishing the new
97 infection of the mosquito by adapting to different nutrient availability, polarizing the cell to regain motility, and initiating
98 zygotic transcription. Notably, this is the first application of quantitative Data Independent Acquisition Mass
99 Spectrometry (DIA-MS) proteomics to *P. yoelii*, which now provides the most comprehensive proteomes of female
100 gametocytes and zygotes for any *Plasmodium* species. These data also reveal changes in post-translational modifications
101 associated with female gametocytes and/or zygotes that could be used to toggle translational control across this
102 transmission event. In addition, we have assessed how the DCA translational repression complex contributes to this
103 regulatory control point. Using both proximity proteomics and high-resolution imaging microscopy, we have assessed
104 potential spatial and/or compositional changes in the complex across the host-to-vector transmission point. Together,
105 this provides the first stage-matched evidence for the widespread activation of translation of repressed transcripts in
106 early mosquito-stage parasites and we posit that changes in the spatial arrangement and composition of DCA complex
107 play important roles in the release of translational repression.

108 **Results:**

109 **Collection of *P. yoelii* Female Gametocytes and Zygotes**

110 In order to compare gene expression between female gametocytes and zygotes, we first enriched these specific life
111 stages using flow cytometry. Female gametocytes were collected from a transgenic parasite line expressing a fluorescent
112 tag (GFP) from a female-enriched promoter (*pylap4*), while *in vitro* cultured zygotes were selected by anti-Pys25
113 antibodies as this protein only becomes surface exposed following fertilization (22). The stage identity of the collected
114 cells was validated by Giemsa-stained thin blood smears and fluorescence microscopy to ensure stage-specific
115 enrichment (Fig S1, S2).

116 **Transcriptomic Profiling of Female Gametocytes and Zygotes**

117 RNA-seq libraries were generated using four million parasites per biological replicate with the Illumina Stranded mRNA
118 Library kit for NextSeq single-read sequencing. The resulting RNA-seq data were mapped to the PY17X reference
119 genome (plasmodb.org, release 55) using hisat2, and differentially abundant transcripts in each stage were identified
120 using DESeq2 with at least a 5-fold difference in abundances (Fig 1, Table S1) (23). Biological replicates are well-
121 correlated by life stage, as demonstrated by stage-specific hierarchical clustering of sample-to-sample distance (Fig 1A).
122 Between these two stages, 2,648 transcripts were detected in total, and nearly all transcripts (92%) detected in
123 gametocytes were also detected in zygotes (Fig 1B), reflective of the transcripts present in the shared cytosol between
124 female gametes and zygotes.

125 Among the 194 transcripts enriched in female gametocytes include those encoding proteins involved in DNA replication
126 licensing, like components of the origin recognition complex (ORC2), and the minichromosome maintenance complex
127 (MCM2, MCM5, MCM6, MCM7) (Fig 1CD, Table S1). Though the female gametocyte does not replicate its DNA, the
128 female gametocyte transcriptome was enriched in enzymes involved in DNA replication like DNA primase, DNA
129 polymerase α and δ subunits, and components of the proliferating cell nuclear antigen DNA clamp (PCNA) and its
130 replication factor C clamp-loader complex. It is likely that the female gametocyte is preparing for the DNA replication
131 activities that occur early on in zygote development when the diploid zygote replicates its DNA to become tetraploid
132 within the first hours following fertilization (10, 14, 24). Of note, many previously identified female-enriched transcripts
133 were abundantly detected in both female gametocytes and zygotes, with no statistically significant difference in
134 transcript abundance (*nek4*, *dozi*, *cith*, *p28*) or even a greater abundance in zygotes (*lap1*, *lap3*, *p25*).

135 Together, these data are consistent with the proactive transcription, storage, and stabilization of some transcripts in the
136 female gametocyte, as well as *de novo* transcription in the early zygote that is activated by two essential transcription
137 factors, first by the recently identified ApiAP2-Z and then by ApiAP2-O (11, 13, 25). This strategy mirrors that of the

138 metazoan maternal-to-zygotic transition, especially as these two *Plasmodium* ApiAP2 factors are known to be
139 translationally repressed in female gametocytes, and translated early in mosquito stage development to contribute to
140 zygotic genome activation following fertilization (11, 13, 25). Many of the 685 transcripts that are differentially abundant
141 in zygotes have been identified as target genes bound by *P. berghei* ApiAP2-O in ookinetes that develop from zygotes
142 (Figure 1CD, Table S1), including the transcript for the zygote and ookinete surface protein Pbs28, one of the best
143 studied, translationally repressed transcripts in female gametocytes (9, 25). Additionally, ChIP-seq targets of PbApiAP2-Z
144 or PbApiAP2-O were also found to be more abundant in zygotes, including those that encode proteins involved in
145 ookinete morphological development and secreted ookinete proteins involved in midgut traversal and ookinete-to-
146 oocyst differentiation, such as *celtos*, *soap*, *warp*, *chitinase*, and perforin-like proteins *plp3*, *plp4*, *plp5* (Fig 1E) (11, 25).
147 Many members of the IMC also have increased transcript abundance in zygotes, including IMC1 subunits and IMC sub-
148 compartment protein ISP3. Together, these data support zygotic genome activation at this early timepoint and align
149 with the reported roles of these ApiAP2 transcription factors in zygote-to-ookinete maturation.

150 **Establishment of Data Independent Mass Spectrometry (DIA-MS) for *Plasmodium yoelii***

151 Next, we applied DIA-MS proteomics in order to measure the relative protein expression between female gametocytes
152 and zygotes. We employed a data acquisition and library-building strategy developed by Searle and colleagues (26).
153 Unlike traditional data-dependent acquisition (DDA), in which peptide precursor ions are sampled in a serial fashion,
154 DIA-MS fragments peptide ions over sequential wide bands of mass-to-charge ratios, thus removing DDA's bias toward
155 random high-abundance precursors and providing the opportunity to quantify more of the peptides present in a sample.
156 In addition to providing deep proteome detection and robust quantification even from scarce samples, DIA-MS is well-
157 suited to analyze obligate parasites as it is much less sensitive to interference from contaminating host proteins (26). In
158 order to deconvolute complex spectra generated by fragmentation of wide *m/z* windows, DIA-MS data is typically
159 searched against a spectral library, which is a compendium of MS/MS spectra for individual peptides generated from
160 DDA experiments. In order to create the requisite comprehensive spectral libraries for our analysis beyond our
161 empirically derived spectral data, we used Prosit (27), a deep neural network trained on millions of peptide spectra, to
162 create *in silico* reference spectra for all theoretical tryptic peptides of the *P. yoelii* and mouse proteomes. To produce
163 sample-specific spectral libraries tailored to the specific chromatography and MS instrumental conditions, we produced
164 representative female gametocyte and zygote samples in sufficient quantity to enable six replicate injections of each.
165 We then used gas-phase fractionation DIA (28), a DIA-MS technique in which narrow ranges of *m/z* are fragmented in
166 each replicate injection, enabling deep proteome coverage without requiring offline pre-fractionation. The resulting
167 spectra from these experiments were searched against the Prosit *in silico* spectral library and used to build empirically
168 corrected chromatogram libraries for which the retention time and peptide fragment spectra have been empirically
169 determined using the same experimental conditions used to generate the sample data to be searched (29). These

170 empirically corrected spectral libraries therefore enable the quantification of more peptides than from a Prosit library
171 alone (26).

172 Although the purpose of the empirically derived chromatogram libraries was to provide deeper proteomic coverage for
173 the six gametocyte and zygote biological replicate samples with matched transcriptomic data, the libraries themselves
174 provide valuable insight into protein expression of these parasite stages, especially since the proteome coverage
175 enabled by gas-phase fractionation was deeper than could be obtained from the limited material available from the
176 individual samples. A total of 3358 *P. yoelii* proteins were quantified from the combined female gametocyte and zygote
177 library samples: 2388 from gametocyte and 3184 from zygote, with 2214 quantified in both (Fig 2A, Table S2). Each
178 library sample represents only a single biological replicate, but by applying conservative thresholds for differential
179 expression, we identified proteins that likely represent stage-specific protein expression. In addition to providing
180 confirmatory evidence for the stage-specific protein expression identified from the transcriptomics-matched biological
181 replicates, this library data set represents a valuable resource to the *Plasmodium* research community as it provides the
182 most comprehensive *P. yoelii* gametocyte proteome to date and the first zygote proteome reported for any *Plasmodium*
183 species.

184 **Quantitative Proteomics by DIA-MS**

185 Compiling the results of the library and samples and comparing them against the current body of published *Plasmodium*
186 proteomes compiled in PlasmoDB (23) provides new insights into stage-specific protein expression (Table S2, Table S3).
187 Relatively few comprehensive proteomes have been published for *P. yoelii* at any stage, so we also compared our results
188 against published *P. falciparum* proteomes for proteins annotated as orthologs in PlasmoDB. Altogether, this
189 compendium of *Plasmodium* proteomics includes data from one *P. yoelii* (30) (not in PlasmoDB) and 34 *P. falciparum*
190 asexual stage samples, seven *P. falciparum* gametocyte samples, five *P. yoelii* and 20 *P. falciparum* sporozoite samples,
191 and two *P. yoelii* liver stage samples. We now add to this list our four samples each of *P. yoelii* gametocytes and zygotes.
192 Parsing these results reveals 276 *P. yoelii* proteins (145 of which have annotated *P. falciparum* orthologs) that were
193 confidently identified in zygotes by at least two peptides, but for which no proteomic evidence has been detected in any
194 other stage in *P. yoelii* or *P. falciparum*, representing a set of stage-specific protein markers for early mosquito stages.
195 Among these are several known markers of this class, including members of the PSOP secreted ookinete proteome
196 family (31), members of the CPW-WPC family of translationally repressed ookinete proteins (32), chitinase (CHT1, an
197 ookinete protein essential for invasion of the mosquito midgut (33)), and the ookinete surface protein WARP (33, 34).
198 Notably, 142 of these putative stage-specific proteins have no annotated function, representing a short list of targets for
199 future studies to identify proteins that are essential for transmission and could thus be targetable via transmission-
200 blocking vaccine approaches.

201 As with our transcriptomic data, biological replicates of the sample DIA-MS datasets clustered well by stage (Fig 2B). A
202 comparison of protein abundance across stages identified many proteins with significantly different abundance levels or
203 that were only detected in one of these stages (Fig 2C). A total of 550 proteins met the criteria to be considered
204 significantly more abundant in female gametocytes (protein signal >25th percentile and detected only in gametocytes, or
205 with a ratio>5-fold and p-value < 0.05). Among these are the ApiAP2-G2 regulator of gametocyte maturation (35),
206 proteins important for gamete egress such as PPLP2, MTRAP, SUB1 and 2, and GEST, and the gamete surface proteins
207 (and transmission-blocking vaccine antigens) P48/45 and P230 (Fig 2C). Similarly, proteins required for licensed DNA
208 replication that were also more abundant at the RNA level in female gametocytes were also differentially abundant.
209 These include ORC1-5, Cdt1, CDC6, MCM2-7, MCMBP, as well as DNA primase, TOPO 1 and 2, mismatch repair enzymes,
210 FANCJ-like helicases, RUVB1-3, and many members of the DNA polymerases alpha, delta, and epsilon, and the clamp
211 loader complexes. In contrast, the 632 differentially expressed proteins in zygotes (same thresholds applied) include
212 those involved in key early mosquito stage events. Among the most abundant up-regulated zygote proteins are
213 members of the LCCL-domain containing family (CCp and LAP (36, 37)), which are essential for the maturation of
214 gametes and ookinetes. Unlike in typical metazoans, meiosis in *Plasmodium* occurs after fertilization (38), and
215 accordingly, we detected key meiosis proteins in the zygote, including NEK4, DMC1, and RAD51. Additionally, we detect
216 proteins required by early mosquito-stage parasites to become motile (IMC proteins and their regulators, CelTOS),
217 adjust their surface protein composition (p25, p28, PSOPs, CPW-WPCs, CTRP, WARP, all known members of the
218 crystalloid), develop the ability to evade mosquito immunity (P47, Cap380), and prepare for segmentation (basal
219 complex members). We also detected an increased abundance of NOT5, which plays a role in engaging translating
220 ribosomes encountering non-optimal codons in the A-site (39). Moreover, we observed that key components of the
221 mitochondria are differentially abundant, including much of the respiratory chain (Complexes III, IV, and ATP synthase),
222 and associated transporters required for their function are differentially abundant in zygotes, reflecting the need to
223 rapidly adapt to the lower nutrient availability of mosquitoes. In addition, transcriptional regulators ApiAP2-Z, O, and O2
224 are differentially abundant in accordance with their known, essential roles in early mosquito stage development. Finally,
225 we surprisingly observed that the protein abundances for both DOZI and CITH increased in zygotes, suggesting that they
226 may play continuing roles in mosquito stage development.

227 **Identification of 198 Translationally Controlled mRNAs Across the Host-to-Vector Transmission Event**

228 Previous comparative transcriptomic and proteomic analyses of female gametocytes identified transcripts with high
229 mRNA abundances but disparate protein abundances (6, 12). These studies did not examine translation in the
230 subsequent zygote or ookinete stages, and so the widespread release of translational repression has not yet been
231 demonstrated. To identify mRNAs that were translationally repressed in female gametocytes, where this repression was
232 relieved in early zygote stage parasites, we applied several criteria. First, mRNAs must pass transcript integrity (TIN) and
233 minimum read count thresholds as previously described (40). These mRNAs must not increase >5-fold in zygotes versus

234 female gametocytes, as substantial increases in mRNA abundance due to the start of zygotic genome activation could
235 explain comparable increases in protein abundance. These gates yielded 1417 mRNAs for these comparisons (Table S4).
236 Second, proteins detected by data-independent acquisition (DIA) proteomics must either be detected only in zygotes, or
237 must change >5-fold in zygotes versus female gametocytes. Additionally, we imposed a conservative abundance
238 threshold (>25th percentile) to ensure that fold-change values are robust. These thresholds yielded 649 proteins for this
239 analysis (Table S4). The union of these mRNA and protein lists identified 198 mRNAs that are translationally repressed in
240 female gametocytes, with a subsequent release of translational control early in zygotes that permits substantial
241 translation of the protein (black dots in Figure 3A, Table S4).

242 Of the 198 mRNAs that are subject to translational repression in the female gametocyte that is relieved in the early
243 zygote, there is an overrepresentation of mitochondrial proteins that function in the respiratory chain (Complexes III and
244 IV, ATP synthase) (41), as well as related metabolic enzymes and carrier proteins. This is reflected in all three categories
245 of GO term analyses that note statistically significant terms related to the respiratory chain, active transport across the
246 inner mitochondrial membrane, oxidative phosphorylation, and more (Table S4). This prioritization of mitochondrial
247 functions is consistent with the parasite's requirement to change modes of energy production away from glycolysis
248 during asexual blood stage growth in the glucose-rich environment of the mammalian host. While the shift toward the
249 use of the respiratory chain begins during gametocytogenesis (42), these data indicate that specific components or
250 overall reliance are required to a greater extent in zygotes in the more restrictive environment of the mosquito, even
251 while still bathed in the blood meal. This finding aligns with data indicating that efficient, full respiration is required for
252 mosquito stage development, and that atovaquone treatment of mosquitoes causes arrest of parasites at the zygote
253 stage (43, 44).

254 In addition to escalating mitochondrial functions, these translationally repressed mRNAs also include those that produce
255 proteins that are critical for core ookinete functions. These include known surface and secreted proteins of zygotes and
256 ookinetes (p28, PSOP family proteins), regulatory proteases (plasmepsins VII and VIII), as well as many of the known
257 crystalloid proteins (e.g., PH-like proteins, MOLO1, NTH, and CPW-WPC proteins) (45). This aligns with previous
258 publications that identified these mRNAs as being translationally repressed in single-gene studies (reviewed in (19, 46)).
259 Additionally, this group includes 27 members of the glideosome/inner membrane complex required for ookinete
260 development and motility (e.g., GAPM1, GAPM2, GAP40, GAP50, IMC1b,d,h) ((47-49), and reviewed in (50)). *De novo*
261 IMC formation is essential in order to initiate and extend a protrusion as the zygote first becomes a retort and develops
262 further into the elongated, motile ookinete (reviewed in (51)). Importantly, two palmitoyltransferases (DHHC3 and
263 DHHC7) known to be an IMC resident protein were also identified as being translationally repressed. DHHC3 has been
264 shown to contribute strongly to ookinete motility, and disruption of its gene leads to a correspondingly severe decrease
265 in the intensity of oocyst numbers (52). Moreover, DHHC7 is known to be an IMC resident of asexual blood-stage
266 parasites, where its palmitoylation activity can be directed toward IMC members (47).

267 Interestingly, the mRNAs of DOZI and CITH are also translationally repressed, albeit incompletely, as their protein
268 abundance continues to increase as zygotes are formed. While it is not known if DOZI and CITH continue to contribute a
269 function to the parasite beyond its essential activities in the early zygote due to their complete arrest in this stage, these
270 data would suggest that perhaps they might. Finally, the mRNA for the meiotic recombination protein DMC1 is also
271 under this translational control. This is notable, as deletions of *pbdmc1* have no phenotype prior to early mosquito stage
272 development, which first presents with a substantial decrease in both the number and size of the resulting oocysts (53).

273 In addition, only one ApiAP2 protein was produced upon the release of translational repression: ApiAP2-Z. These
274 findings are in agreement with recent reports that defined ApiAP2-Z as being critical for zygotic functions, and is likely
275 the initial driver of transcription during zygotic genome activation (11). In addition, several uncharacterized zinc finger
276 proteins and RNA-binding proteins could feasibly contribute to translational control and/or zygotic genome activation.
277 Together, these results align with the time-sensitive requirements that zygotes must meet in order to productively infect
278 the mosquito (reviewed in (54)).

279 **Additional Features of Stage-Dependent Gene Expression**

280 We also identified transcripts and proteins with increased abundances in either gametocytes or zygotes (Fig 3A). The
281 gene products in this plot's lower left section are abundantly expressed in female gametocytes over zygotes (Fig 3A,
282 Table S4). This includes proteins involved in DNA licensing and replication, like DNA licensing factors MCM2-7 and MCM-
283 BP, DNA primase subunits, replication factor C subunits, and DNA polymerases (α, δ, ε). These proteins in female
284 gametocytes are likely generated in preparation for the early DNA replication following parasite transmission and
285 fertilization in the mosquito midgut. In contrast, some of the most abundant and best-characterized proteins of early
286 mosquito stage development can sufficiently rely upon *de novo* transcription following the start of zygotic genome
287 activation (ZGA) (Fig 3A upper right quadrant, Tables S2, S3, S4). In addition, proteins that will be important later in
288 mosquito stage development are also in this quadrant, such as the oocyst capsule protein Cap380, inner membrane
289 complex proteins important for the structure of ookinetes as they develop (IMC1c, e, i, j, k), ookinete surface expressed
290 proteins P47 and P25, secreted ookinete proteins WARP and perforin-like protein 4, and additional components of the
291 mitochondrial electron transport chain (e.g., members of the cytochrome b-c1 complex, complex II subunits, and ATP
292 synthase subunits F0, O, δ, and ε). Some of these transcripts are abundantly expressed in female gametocytes as well,
293 but the increase in transcript abundance and protein abundance in zygotes highlights the importance of their expression
294 ahead of ookinete development.

295 Finally, it is important to note that many of these abundant mRNAs do not have their encoded protein detected in either
296 stage. This could indicate that the proteins are not detectable despite the presence of tryptic peptides that could
297 reasonably be detected by mass spectrometry (Table S4). Alternatively, these mRNAs could remain under translational

298 control beyond this early zygote timepoint to enable protein production at a later time in early mosquito stage
299 development. In agreement with this possibility, one of these transcripts (*limp*) has been shown to be transcribed in
300 starting in gametocytes and only becomes translated in ookinetes (55). We anticipate that other comparably regulated
301 transcripts experiencing extended translational repression also are found in this dataset.

302 **Comparison of Translationally Repressed *P. yoelii* mRNAs to *P. falciparum* and *P. berghei* Datasets**

303 We next compared the proteins identified in our list of translationally repressed transcripts to previously identified
304 putatively repressed transcripts in *P. falciparum* female gametocytes (Fig 3B) (6). Many of the putatively translationally
305 repressed transcripts identified in *P. falciparum* female gametocytes were found to be abundantly expressed as proteins
306 in *P. yoelii* zygotes (pink datapoints in Fig 3B), and a little over a third (70) of the 198 transcripts we found to be
307 translationally repressed were also identified as putatively repressed in *P. falciparum* gametocytes (6). This underscores
308 the conservation of translational control over core developmental processes across *Plasmodium* species. Next, we
309 compared our data to transcripts associated with PbDOZI in female gametocytes (21). We observed many that were
310 abundantly detected as protein in zygotes, but also a proportion had no difference in protein abundance between
311 gametocytes and zygotes, or even greater abundance in female gametocytes (blue datapoints in Fig 3C). This list of
312 putatively translationally repressed transcripts of *P. falciparum* female gametocytes more closely clusters with the
313 translationally repressed transcripts identified in our *P. yoelii* comparative study than those transcripts bound by
314 PbDOZI. This observation may reflect the presence of non-specifically interacting RNAs in the native RNA
315 immunoprecipitation experiment with PbDOZI that did not utilize crosslinking and highly stringent wash conditions.
316 Moreover, this may indicate that additional transcript-specific translational controls that are independent of DOZI may
317 be present in female gametocytes.

318 **Changes to the DOZI/CITH/ALBA Complex Across the Host-to-Vector Transmission Event**

319 In order to determine mechanisms that may control translation across host-to-vector transmission, we assessed the
320 composition of the DOZI/CITH/ALBA (DCA) translationally repressive protein complex before and after transmission. We
321 and others have identified components of the DCA complex in *P. yoelii* and *P. berghei* via IP/MS in asexual blood stages,
322 gametocytes, and oocyst sporozoites either with or without crosslinking (7, 10, 20). However, it was not clear how the
323 DCA complex may respond to transmission cues that are predicted to cause the release of its bound and regulated
324 mRNAs and thus relieve translational control.

325 Therefore, we employed proximity proteomics by fusing a variant of *E. coli* biotin ligase and GFPmut2 to the C-terminus
326 of DOZI and ALBA4 as experimental bait proteins, or as an unfused control to account for highly abundant proteins in the
327 same compartment (i.e., cytosol) (Fig S3, S4A). We chose this approach to not only determine the protein composition
328 of the DCA complex across host-to-vector transmission, but also to determine if spatial organization of this complex

329 changes. We selected DOZI and ALBA4 as they are known to associate with the 5' or 3' end of bound mRNAs,
330 respectively (10, 20, 56), and thus provide protein proxies for the two ends of target mRNAs. We initially tested the first-
331 generation BioID enzyme before adopting the use of the further engineered TurboID (TID) ligase that allowed for more
332 robust labeling in a shorter labeling time, as we and others have recently shown for *P. falciparum* and *P. berghei* (Fig
333 S4BC) (47, 57-61). To establish an appropriate duration of labeling, we assessed *in vivo* biotinylation with
334 supplementation with 150 µM biotin for increasing time, then used total parasite lysate for affinity blots probed with
335 streptavidin-HRP for both bait parasite lines, ALBA4::TurboID::GFP and DOZI::TurboID::GFP (Fig S4B-F). We found that
336 one hour of biotin supplementation was sufficient for robust biotin labeling by TurboID in total parasite lysates for both
337 female gametocytes and zygotes. Therefore, we used these labeling conditions for all experiments and analyses
338 described here.

339 Biotinylated proteins were able to be captured from female gametocyte or zygote lysates on magnetic streptavidin
340 beads for on-bead tryptic digestion and mass spectrometry analysis (Fig S4G-K). Biotinylated proteins proximal to either
341 bait protein were captured, and their identities were inferred from peptides detected by tandem mass tag-mass
342 spectrometry (TMT-MS) for quantitative analyses. The abundance of detected proteins was normalized to the
343 abundance of proteins detected in cytosolic, unfused TurboID experiments to account for any non-specific biotinylation.
344 Detected proteins greater than four-fold enriched over the unfused control were considered enriched interactors of
345 DOZI or ALBA4 bait proteins. Three biological replicates of TurboID experiments were prepared for each bait or control
346 protein in both gametocytes and zygotes. With these datasets, we next made a comparison of protein interactions
347 between bait proteins and across life stages to changes to the complex pre- and post-fertilization (Table S5).

348 By first comparing DOZI's or ALBA4's interacting partners in gametocytes and zygotes, we observed that proteins
349 proximal to either protein changed substantially across the host-to-vector transmission event (Fig 4AB). Few protein
350 interactions remained consistent between female gametocytes and zygotes, with only 14 proteins associated with
351 ALBA4 in both gametocytes and zygotes, while only 13 interacted with DOZI in both life stages (Fig 4CD). The 14 stage-
352 independent interactors of ALBA4 included ALBA-family proteins ALBA1 and ALBA2, poly(A)-binding proteins PABP1 and
353 PABP2, and RNA-binding proteins HoMu, GBP2, and DDX1, whereas the stage-independent interactions of DOZI included
354 known interactor eIF4E and RNA-binding protein CELF2. The remaining protein interactions of DOZI and ALBA4 were
355 stage-dependent, and perhaps these differences correspond to distinct functions in mRNA regulation in each life stage.
356 In gametocytes, ALBA4 also interacted with proteins involved in translation at both the 5' and 3' end of transcripts, such
357 as small and large ribosomal subunit proteins, initiation factors eIF4A, eIF4G, eIF3A, and RNA-binding proteins DOZI,
358 CITH, CELF1 and CELF2, and DBP1. These associations were lost in zygotes when ALBA4 shifted to interact with proteins
359 found at the 3' end of mRNAs, including PABP1 (cytosolic) and PABP2 (nuclear), as well as ALBA1, ALBA2, GBP2, DDX1,
360 DDX5, HoMu/Musashi, UPF1, and ribosomal proteins of both the large and small subunits.

361 We observed that DOZI also interacted with proteins found at either the 5' and 3' end of transcripts in female
362 gametocytes, as well as RNA-binding proteins CITH, ALBA1 and ALBA3, factors involved in mRNA decapping (Dcp1,
363 Dcp2), many members of the major deadenylation complex CAF1/CCR4/NOT complex (CCR4-1, CAF1, CAF16, NOT2, and
364 NOT1-G), regulators of translation (eIF2, eIF3, eIF4E, eIF6), a homolog of ataxin-2 and the recently described FD1 RNA-
365 binding protein (62). However, DOZI was no longer proximal to these proteins in zygotes. Most notably, DOZI exchanges
366 its interaction with NOT1-G for one with its paralogue, the canonical NOT1 protein. Of these paralogues, only NOT1 has
367 a bioinformatically predictable domain known to stimulate the ATPase activity and concomitant release of RNA by
368 DOZI's orthologues in model eukaryotes (63). These findings indicate that NOT1-G and NOT1 proteins form distinct
369 complexes in gametocytes and zygotes, respectively, which aligns with the essential functions of NOT1-G in gametocytes
370 and may contribute to an mRNA-release mechanism (40).

371 We next compared the interactions of DOZI and ALBA4 between each other to compare changes to the complex pre-
372 and post-fertilization (Fig 4). Nearly two-thirds (62%) of the proteins proximal to ALBA4 in gametocytes were also
373 proximal to DOZI at this stage, including many proteins known to bind to the 5' or 3' ends of mRNAs (Fig 4C). This
374 indicates that DOZI/CITH/ALBA mRNPs adopt a condensed conformation during translational repression in female
375 gametocytes. This condensed complex includes reciprocal labeling of DOZI and ALBA4, as well as mutual labeling of RNA-
376 binding proteins (CITH, GBP2, CELF2, PABPs, ALBA1, PUF1, DDX1), large subunit ribosomal proteins, translation initiation
377 factors (eIF3 subunits, eIF4A, eIF4G), GEP, and casein kinase 2A. Detected interactions-of-note are represented in the
378 schematic in Fig 4CD, in which we also incorporated previously reported IP-MS data for these proteins into our protein
379 network to indicate cross-validating data. Many previously reported interactions of DOZI or ALBA4 were also detected
380 here by TurboID in gametocytes, including all previously detected PbDOZI core interactors identified by native IP-MS (Fig
381 S5). In contrast, very few previously identified interactors of DOZI or ALBA4 were detected in the zygote stage by
382 TurboID, and not many proteins were detected as interactors of both ALBA4 and DOZI at this stage (Fig 4). In fact, ALBA4
383 and DOZI are not reciprocally labeled in zygote stage experiments, consistent with the dissolution and/or spatial
384 rearrangement of this complex into distinct 5' and 3' subcomplexes after the complex's role in transcript stabilization
385 and translational repression in gametocytes is completed.

386 Taken together, the compositional and spatial rearrangements detected by proximity proteomics are consistent with
387 DOZI/CITH/ALBA mRNPs 1) adopting a condensed state during translational repression in female gametocytes, and then
388 2) undergoing composition changes that promote its elongation in zygotes following the release from translational
389 repression. These data align with recent smFISH and KARR-seq studies of mRNA compaction in model eukaryotes that
390 reached similar conclusions (64-67).

391 **Validation of Protein Colocalization by Ultrastructure Expansion Microscopy and Structured Illumination Super-**
392 **Resolution Microscopy**

393 To further investigate subcellular protein interactions detected in the condensed DCA storage granules present in female
394 gametocytes, we assessed the colocalization of protein interaction pairs by ultrastructure expansion microscopy as it
395 now routinely enables sub-100nm resolution (U-ExM, Fig 5) (68, 69). We enriched PyDOZI::GFP female gametocytes as
396 above and stained expanded parasites with antibodies against GFP and either PyCITH, PyPABP1, or PyALBA4. We
397 observed extensive colocalization of DOZI with all three proteins in classic cytosolic puncta (pink = colocalization) (Fig 5)
398 (20, 70, 71). Furthermore, to enumerate the colocalization of each antibody pair, we used structured illumination super-
399 resolution microscopy (SIM, Fig S6) to determine their overlap coefficient (0 being no overlap and 1 being complete
400 colocalization) (72) (Fig S6). As with U-ExM, we observed substantial colocalization between DOZI/GFP, ALBA4, and
401 PABP1. In addition, because we detected PyNOT1-G as being proximal to DOZI in female gametocytes, we assessed its
402 colocalization by SIM and also found substantial overlap in its localization with DOZI, ALBA4, and PABP1. Together, these
403 results corroborate the proximity proteomics results and support the presence of a condensed, cytosolic
404 DOZI/CITH/ALBA granule interacting with NOT1-G in female gametocytes.

405 **Notable Post Translational Modifications Detected in Female Gametocytes and Zygotes**

406 Consistent with prior reports, we have identified a wealth of kinases that are expressed in female gametocytes and
407 zygotes (73). Some of these kinases have previously been shown to functionally regulate the essential activities of these
408 stages (74). The quantitative proteomics data we generated in this work did not measure post-translational
409 modifications (PTMs) because the program used to generate the *in silico* spectral libraries used for searching the DIA
410 data is not capable of predicting spectra for peptides bearing PTMs. In order to find evidence of phosphorylation in the
411 proteomic data, we used the DISCO tool from the Trans-Proteomic Pipeline (75) to transform the DIA data into pseudo-
412 DDA data that could be searched for variable modifications using standard shotgun proteomics data analysis tools. Even
413 without the enrichment of phosphopeptides, we qualitatively identified 464 phosphopeptides from 232 proteins (Table
414 S6). Notably, all phosphorylation events on detected glideosome/IMC proteins are only seen in zygotes, with the lone
415 exception being ISP1, which has phosphopeptides only detected in female gametocytes (Table S6). Similarly,
416 phosphorylation of DOZI/CITH/ALBA complex members was skewed to be substantially or only detected in zygotes
417 (Table S6). Of the 177 phosphopeptides detected in proteins associated with DOZI and/or ALBA4 in female gametocytes
418 and/or zygotes, two-thirds (117/177) are only detected in zygotes. These phosphopeptides are detected in DOZI, CITH,
419 CELF2/Bruno, ALBA proteins 1-4, GBP2, PREBP, DBP1/DDX3, eIF3a, eIF4a, PABP1, PAIP1, NOT1-G, CAF16, and GEP.
420 Another 15% of the total (27/177) were observed in both female gametocytes and zygotes. These qualitative data are
421 consistent with a phosphorylation-based regulation of the members of this complex, such as on the positionally
422 conserved Ser20 of DOZI within a predicted intrinsically disordered region in its N-terminus (76). While these findings
423 coincide with the release of its translationally repressive activity, establishing whether and which modifications are
424 causal remains to be determined.

425 **Discussion:**

426 Malaria parasites must detect and respond to environmental cues across their developmental cycle, and perhaps most
427 pressingly, must do so during their two transmission events between host and vector. Failing to quickly respond reduces
428 or eliminates the parasite's ability to persist and perpetuate itself post-transmission.

429 Therefore, *Plasmodium* parasites proactively prepare mRNAs ahead of time so that their encoded proteins can be
430 rapidly produced when needed without the time required for *de novo* transcription to occur. Moreover, this provides an
431 energetically favorable approach to preparation, as the energetic cost of translation is deferred. Together, this just-in-
432 time approach helps the parasite to rapidly initiate the next phases of its development and countermeasures against its
433 host or vector. This scenario mirrors the requirements of a newly fertilized metazoan zygote, which must also rapidly
434 initiate development upon fertilization even before zygotic genome activation (ZGA) and widespread *de*
435 *novo* transcription occurs. To achieve this developmental need, metazoans rely on the process of maternal-to-zygotic
436 (MZT) transition whereby mRNAs are translationally repressed in the female gamete and then translated upon
437 fertilization. In both *Plasmodium* and metazoans, translationally repression of select mRNA is enacted by well-conserved
438 RNA-binding proteins (RBPs) and their partners that localize these mRNAs into cytosolic storage granules.

439 Much has been done to identify the RBPs that govern translational repression in *Plasmodium* parasites (reviewed
440 in (19)). These proteins, such as DOZI, CITH, ALBA family proteins, PUF proteins, and more, constitute a weak point in
441 these essential regulatory functions that can be exploited. In addition, several studies have identified mRNAs that
442 putatively are translationally repressed in female gametocytes or sporozoites. In one recent study, we have also
443 experimentally validated the translational repression and then release of specific mRNAs globally in both *P.*
444 *falciparum* and *P. yoelii* sporozoites (77). These findings revealed that multiple orthogonal programs of translational
445 control can be imposed simultaneously and relieved independently. However, such a global approach had not yet been
446 taken for host-to-vector transmission to assess the release of translational repression during the development of female
447 gametocytes to fertilized zygotes.

448 Therefore, in this study, we have used a multi-omic comparative transcriptomics and the first application of highly
449 sensitive quantitative DIA-MS proteomics to *Plasmodium yoelii* to interrogate the control of gene expression in female
450 gametocytes and zygotes. Several key observations now allow us to understand these stages more clearly. First, our
451 proteomic study of zygotes provides an important and comprehensive proteomic view of this stage. Prior to this work,
452 the only proteome of zygotes was studied by Vinetz and colleagues in 2008 using *P. gallinaceum* without a reference
453 genome for this species (16). Our proteome greatly expands what was detected (3184 vs. 966 proteins) and fills in key
454 details of zygote biology. Second, these data reveal what proteins can be made ahead of transmission in the female
455 gametocyte, and also indicate which proteins cannot. For example, female gametocytes proactively prepare both

456 transcripts and proteins required for licensed DNA replication, although they would not be required until after
457 fertilization. Third, these data indicate what RNAs and proteins can be produced solely after transmission, without the
458 need for the benefits of translational repression of mRNAs. These include several essential ookinete proteins (SOAP,
459 WARP, etc.) that are rapidly transcribed and translated in the early zygote. Many of these differentially abundant mRNAs
460 in zygotes are putative targets of the ApiAP2-Z and ApiAP2-O specific transcription factors, which are subject to
461 translational control presumably to enable rapid *de novo* transcription of these genes (11, 25). Fourth, many abundant
462 transcripts are detected in both female gametocytes and zygotes that were not detected as a protein in either timepoint
463 in our study. This may reflect further repression that is not relieved until later in mosquito stage development (e.g.,
464 ookinetes, oocysts). Moreover, DIA-MS enabled the detection of post-translational modifications without the need for
465 enrichment of these modifications. We observed several differential phosphorylation marks on members of the
466 DOZI/CITH/ALBA complex between female gametocytes and zygotes. In other eukaryotes, such PTMs can promote
467 regulatory events by affecting homotypic oligomerization and non-uniform scaffolding interactions that are used to form
468 and dissolve cytosolic granules (78).

469 Finally, these data reveal 198 mRNAs that are translationally repressed in female gametocytes that are then translated
470 soon after fertilization in zygotes. This enables the rapid production of proteins that are integral to essential processes of
471 the early mosquito-stage parasite, which include the mitochondrial respiratory chain (Complexes III, IV, V) to presumably
472 adapt to the more nutrient-poor conditions of the mosquito, and the inner membrane complex (IMC) required for
473 proper development and polarization of the zygote, retort, and ookinete. Moreover, the translational repression
474 program also enables rapid translation of ApiAP2-Z to promote zygotic genome activation, DMC1 for meiosis, and
475 several well-characterized surface proteins important for ookinete viability and function. Surprisingly, we also found that
476 DOZI and CITH have sustained mRNA expression and increased protein expression in zygotes, suggesting that they may
477 play roles in mosquito stage development, which aligns with the timing of their deletion phenotypes (7, 10).

478 Our data also validate the presumed translational control of mRNAs observed in previous studies (6, 74). In one of these
479 studies, Sebastian and colleagues identified CDPK1 as a regulator of the release of translational repression. Of the 65
480 transcripts that they identified to be controlled by both CDPK1 and the DOZI/CITH complex, only 9 are present in the 198
481 regulated mRNAs identified here. This is in agreement with validation experiments conducted by this group, which
482 identified that not all DOZI/CITH-regulated transcripts were governed by CDPK1. This would suggest that other release
483 mechanisms are present and could substantially contribute to TR release in the early zygote stage. Moreover, we
484 identified mRNAs for which there is no associated protein detected in either female gametocytes or zygotes. One of
485 these mRNAs, *limp*, has been shown to undergo extended translational repression that lasts all the way to the ookinete
486 stage (55). Our dataset indicates that this form of extended translational control is more widespread instead of *limp*
487 being an atypical outlying example. This model is consistent with our previous work that demonstrated the multiple
488 orthogonal programs of translational repression can be imposed and released at different developmental times in

489 sporozoites/early liver-stage parasites (77). Determining why the parasite would enact this complex, energetically costly
490 gene regulatory approach is intriguing, as at face value it is counterintuitive to do so if *de novo* transcription could
491 produce sufficient mRNAs at the time they are needed.

492 In addition, we sought to determine mechanisms by which the essential regulatory DOZI/CITH/ALBA complex responds
493 to cues that promote the release of translational repression of mRNA to which it binds. Using TurboID-based proximity
494 proteomics of DOZI and ALBA4, we found that substantial spatial and compositional changes occur across the host-to-
495 vector transmission event. Our findings align with recent reports using smFISH or KARR-seq that refute the classic
496 closed-loop model of mRNA translation and instead show that the translation of mRNAs correlates with a loss of their
497 condensation in both native and stressed states (64-67). Similarly, our proximity proteomic data are consistent with the
498 model of a condensed mRNP under translational repression in female gametocytes with both 5' and 3' ends of the
499 mRNA being in close proximity, which converts to an elongated state with 5' and 3' ends being spatially distinct during
500 translation in zygotes. Advanced imaging microscopy approaches using both ultrastructure expansion microscopy (U-
501 ExM) and structured illumination microscopy (SIM) provided cross-validation of these proximity proteomics results,
502 which showed extensive colocalization of both 5' and 3' end-binding proteins in female gametocytes. Finally, these data
503 also uncovered a compositional change that this complex undergoes as the parasite develops from a female gametocyte
504 to a zygote. We have recently shown that *Plasmodium* uses the NOT1-G paralogue of NOT1 for essential functions of
505 both male and female gametocytes (40). Here, we found that there is a handoff between these paralogues that could
506 provide a mechanism for translational control and its release that correlates with the timing of the *pynot1-g*$^{-}$ phenotype.

507 Therefore, we propose a model encompassing these multi-faceted approaches used by *Plasmodium yoelii* to promote its
508 efficient host-to-vector transmission (Fig 6). *Plasmodium* selectively represses the translation of 198 mRNAs until after
509 an early point post-transmission when they are necessary, but also permits the production of other proteins ahead of
510 time that presumably are tolerated or not detrimental to the parasite in female gametocytes. The environmental
511 stimulus/stimuli that trigger the release of translational repression is not yet known but results in a substantial
512 reorganization of the DOZI/CITH/ALBA complex from a condensed mRNP to an elongated form when translation occurs.
513 While this explains much of the translational control occurring during the transmission of female gametocytes, multiple
514 lines of evidence indicate that DOZI-independent regulation is also at play. This could allow for multiple tiers of
515 translational release over time, translation of specific mRNAs in distinct sub-localizations to promote co-translational
516 interactions and more. Finally, we hypothesize that these same principles of translational control will apply to other
517 *Plasmodium* species, given the substantial overlap in regulation observed between *P. yoelii* and *P. falciparum* female
518 gametocytes.

519 **Materials and Methods**

520 *Ethics Statement:* All vertebrate animal care followed the Association for Assessment and Accreditation of Laboratory
521 Animal Care (AAALAC) guidelines and was approved by the Pennsylvania State University Institutional Animal Care and
522 Use Committee (IACUC# PRAMS201342678). All procedures involving vertebrate animals were conducted in strict
523 accordance with the recommendations in the Guide for Care and Use of Laboratory Animals of the National Institutes of
524 Health with approved Office for Laboratory Animal Welfare (OLAW) assurance.

525 *Use and Maintenance of Experimental Animals:* Six- to eight-week-old Swiss Webster female mice from Envigo were
526 used for all experiments performed with *Plasmodium yoelii* 17XNL strain parasites and were housed in groups of up to 5
527 animals. All protocols with mice were approved by the Pennsylvania State University Institutional Animal Care and Use
528 Committee (IACUC protocol # 42678), and experiments conformed to the Association for Assessment and Accreditation
529 of Laboratory Animal Care (AAALAC) guidelines. Adherence to the principles of the ARRIVE guidelines was maintained
530 throughout the study.

531 *Generation and Validation of Transgenic Parasite Lines:* Transgenic *Plasmodium yoelii* (17XNL strain) parasite lines were
532 created using conventional reverse genetics approaches with specific targeting regions for double homologous
533 recombination for each tagged line (79). Targeting regions for the coding sequence (CDS) and 3' UTR of target genes
534 were PCR amplified from wild-type Py17XNL genomic DNA and combined into a single amplicon by sequence overlap
535 extension (SOE) PCR. The oligonucleotides used in this study to generate and validate transgenic parasite lines are listed
536 in Table S7. This amplicon was inserted into an intermediate plasmid (pCR-Blunt) for initial sequence verification of the
537 target regions. The targeting regions were then inserted into a final pDEF plasmid vector containing the coding sequence
538 for GFPmut2, or TurboID and GFPmut2, with the *P. berghei* DHFR 3' UTR, and the human DHFR drug resistance cassette
539 (20, 40, 80).

540 The final plasmids were linearized and transfected into Accudenz-purified *P. yoelii* schizonts produced in *ex vivo* cultures,
541 as previously described (20, 40, 79-82). Schizonts were transfected with 5-10 ug linearized plasmid using an Amaxa
542 Nucleofector 2b device using cytomix with Program T-016. Electroporated cells were injected into the rodent host by tail
543 vein injection, and parasites were selected by pyrimethamine drug cycling in the initially injected mouse ("parental").
544 Pyrimethamine (ICN Biomedicals Inc., Cat# 194180) was dissolved to 281.4 µM in the mouse drinking water and was
545 provided to the parental mice *ad libitum* starting one day after transfection. The parental mice were provided
546 pyrimethamine drinking water for three days, then were cycled off to regular (no drug) drinking water for at least three
547 days until the parasites were transferred to a second mouse ("transfer") after reaching 1% parasitemia in the parental
548 mouse. Parasites in the transfer mouse were similarly pyrimethamine cycled to select for transgenic parasites, and
549 parasites were collected by cardiac puncture when infection reached 1% parasitemia. Long-term freezer stocks of

550 collected parasites were prepared by mixing 100 uL of collected blood with 400 uL Freezing Solution (9:1 Alsever's
551 solution (Sigma-Aldrich, Cat#A3551):glycerol), and stored in liquid nitrogen. Parasite genomic DNA was purified from the
552 blood of a transfer mouse using the Qiagen QIAamp DNA Blood Kit (Qiagen, Cat# 51106), and genotyping PCR was
553 performed to assess integration into the target locus. In some cases, transgenic parasite populations were enriched over
554 remaining wild-type parasites using FACS to select fluorescent parasites.

555 *Enrichment of Female Gametocytes and Zygotes by Flow Cytometry:* Transgenic parasites that express GFP in a stage-
556 enriched manner in female gametocytes or zygotes, respectively, were used for flow cytometry-based enrichment of
557 these parasite stages. A parasite line driving GFP with a female-enriched promoter, *pylap4*, from a dispensable genomic
558 locus (*p230p*) was used to generate the female-enriched samples (22). Blood from mice infected with this *pylap4* prom-
559 GFP parasite line was collected by cardiac puncture as the infection reached 1-3% parasitemia, as measured by Giemsa-
560 stained thin blood smear. The collected blood was maintained at 37°C to prevent gametogenesis, and infected red blood
561 cells were enriched by Accudenz gradient, as described below. Cells collected from the interface of the gradient were
562 filtered before FACS collection of GFP-positive cells on the Beckman Coulter MoFlo Astrios EQ Cell Sorter. Uninfected
563 blood was used as a background fluorescence control. The collected parasites were also maintained at 37°C before they
564 were combined and pelleted at 200 *xg* for 10 minutes at 37 ºC or 1034 *xg* for 20 minutes at 37°C. From each replicate
565 sort, between 4 and 8 million female gametocytes were collected and stored in 2 million cell aliquots at -80°C for
566 downstream RNA isolation and total proteomic analyses.

567 Zygotes were enriched using a transgenic parasite line expressing PyApiAP2-O::GFP and staining with a zygote-specific
568 antibody, anti-Pys25 (Mm, Mab). Mice infected with PyApiAP2-O::GFP tagged parasites were euthanized as they reached
569 1-3% parasitemia, and blood was collected and maintained at 37°C to prevent premature gametogenesis. Zygotes were
570 cultured as described below, and in the final two hours of zygote culturing, were incubated with anti-Pys25 primary
571 antibody for one hour, then Goat anti-Mouse IgG Alexa Fluor 594 (Invitrogen, A11005) for the final hour. Nuclei were
572 stained with DRAQ5 (Thermo Scientific, Cat # 62251) before cells were pelleted and filtered for sorting on the Beckman
573 Coulter MoFlo Astrios EQ Cell Sorter for Pys25-positive and DRAQ5+ cells. Uninfected blood was used as a background
574 fluorescence control. For each replicate sort, between 4 and 8 million zygotes were collected and stored in 2 million cell
575 aliquots at -80ºC for downstream RNA isolation and total proteomic analyses.

576 *RNA-seq Sample Preparation and Data Analysis:* RNA from FACS-collected female gametocytes or zygotes was prepared
577 using the Qiagen RNeasy Kit (Qiagen, Cat#79254) with in-solution DNaseI treatment (Sigma-Aldrich, Cat# AMPD1-KT).
578 RNA quality was assessed by NanoDrop, RNA quantity was determined by Qubit, and RNA integrity was measured by
579 Bioanalyzer. Samples were used to create barcoded libraries using the Illumina Stranded mRNA kit, and an equimolar
580 pool of the samples was sequenced on an Illumina NextSeq to yield 150 nt long single-end reads for each biological
581 replicate. Data was trimmed to remove the low-quality bases and adapter sequence using fastp (0.22.0). Reads shorter

582 than 35 bp after trimming were filtered out. Data quality was inspected by generating FastQC reports before and after
583 trimming. The trimmed reads were mapped to the *P. yoelii* 17X strain reference genome (Plasmodb.org, release 55)
584 using hisat2, version 2.1.0 (83) specifying '--rna-strandness R' and '--max-intronlen 1500'. Coverage files were generated,
585 and mapping was visualized in Integrative Genomics Viewer (IGV). Reads mapping to the genes were counted with
586 featureCounts (version 2.0.1) (84). Parameters '-t exon -s 2 -g gene_id' were specified for featureCounts. The Transcript
587 Integrity Number (TIN) was calculated to check the integrity of the transcripts as previously described (40). A complete
588 description of commands used in this analysis is provided in the Makefile (File S1). RNA-seq files are available through
589 NCBI GEO (GSE231838; GSM7304682- GSM7304686).

590 Read counts were normalized and differential expression between female gametocytes and zygotes was determined
591 using DESeq2 package in R (85). Reads were filtered for quality by transcript integrity number (TIN) to ensure reads have
592 even coverage across the entire length of the gene (40, 86). For filtering, significantly expressed genes with FDR <0.05
593 and an average TIN <40 in both conditions but with an average count >20 in either of the conditions were flagged for
594 further inspection. TIN-log2-fold change was calculated, and the flagged genes were resolved and included in the
595 differential expression set if the absolute value of TIN log2-FC is < 1.5. The average read counts for transcripts that meet
596 the TIN cut-off were used to calculate the fold change for each transcript detected (average count zygote / average
597 count gametocyte). Transcripts with log2(fold change) > 2.3 were considered to be differentially expressed in zygotes,
598 and those with log2(fold change) < -2.3 were considered differentially expressed in gametocytes. Transcripts detected in
599 either stage were ranked in abundance based on average read count. Heatmaps were generated using DEseq2
600 normalized counts for differentially expressed genes that were converted to a z-score to denote how far the values
601 deviate from the mean. A positive value (shown in red) indicates upregulation in zygotes, and a negative value (shown in
602 green) indicates downregulation in zygotes. A PCA plot was generated with the plotPCA function available in DESeq2
603 package, using VST with transformed raw counts as the input.

604 *Proteomics Sample Preparation:* From each of the six gametocyte and zygote biological replicates analyzed by
605 transcriptomics, an aliquot containing 2 million cells was taken for proteomics. One additional sample of 6M cells of
606 zygotes or gametocytes was prepared for the purpose of creating sample-specific spectral libraries. The cells were
607 washed three times with incomplete RPMI, and the pellet in ~30 µL of media was stored at -80°C.

608 Sample processing for proteomics was carried out using S-Traps (ProtiFi) (87). Unless otherwise noted, all solid reagents
609 were from Merck-Sigma; solvents and acids were Optima LC-MS grade from Fisher Scientific. Water was LC-MS grade
610 from Honeywell Burdick & Jackson. To each cell pellet of ~30 µL was added 30 µL of 10% w/v sodium dodecyl sulfate in
611 100 mM ammonium bicarbonate (ABC) and 2.6 µL 120 mM tris(2-carboxyethyl)phosphine (TCEP, Pierce Bond Breaker) in
612 50 mM ABC. Samples were incubated for 5 min in a 95°C water bath with occasional vortexing, after which they were
613 cooled to room temperature and centrifuged 2 min at 20,000 × *g*. The volume was estimated by pipetting and additional

614 water was added to achieve a final volume of 62.6 µL, then 2.6 µL of 0.5 M iodoacetamide in 50 mM ABC was added,
615 and the samples were incubated for 20 min in darkness at room temperature with vortexing. Samples were acidified by
616 adding 6.5 µL of 27.5 % v/v phosphoric acid and the protein was precipitated by adding 430 µL of S-Trap buffer (90% v/v
617 methanol, 100 mM Tris pH 7.0). Protein was loaded onto S-Traps by adding precipitate suspension in 100 µL increments
618 and centrifuging 30-60s at 1500 *× g.* The traps were washed three times with 150 µL S-Trap buffer and placed in clean
619 1.5 mL microcentrifuge tubes (Eppendorf Protein LoBind). Then 20 µL of 50 mM ABC containing 1 µg of trypsin (Promega
620 Platinum Mass Spectrometry Grade) was added and the traps were incubated 2h at 47°C in a covered thermomixer
621 without vortexing. After digestion, 40 µL of water was added to the traps and peptides were recovered by centrifuging.
622 Two additional recovery washes were performed and combined with the first wash: 40 µL of 0.2% formic acid (FA) and
623 30 µL 50% acetonitrile (ACN). The combined eluates were dried in a vacuum concentrator and resuspended in 20 µL 0.1
624 % trifluoroacetic acid (TFA).

625 *LC-MS:* LC was performed with an EASY-nLC 1000 (Thermo Fisher Scientific, USA) using a vented trap set-up. The trap
626 column was a PepMap 100 C18 (Thermo Fisher Scientific #164946) with 75 µm ID and a 2 cm bed of 3µm 100 Å C18. The
627 analytical column was an EASY-Spray column (ThermoFisher Scientific #ES804) with 75 µm ID and a 15 cm bed of 2µm
628 100 Å C18 operated at 35°C. The LC mobile phases (Honeywell Burdick & Jackson) consisted of buffer A (0.1 % v/v formic
629 acid in water) and buffer B (0.1 % v/v formic acid in ACN). The separation gradient, operated at 300 nL/min, was 4 % B to
630 28 % B over 85 min, 28% B to 30% B over 5 min, 30% B to 80% B over 5 min, and 10 min at 80% B. Prior to each run, the
631 trap was pre-conditioned with 5 µL buffer A at 800 bar, the column was preconditioned with 3.5 µL buffer A at 800 bar,
632 and the sample was loaded onto the trap with 15 µL buffer A. DIA-MS was performed using a Thermo Fisher Scientific
633 Orbitrap Eclipse. The six biological replicate samples were analyzed by a tSIM method with the following acquisition
634 settings: MS1 scan from 395-1005 *m/z* at 30,000 resolution, default AGC settings (target of 4×10^5 ions, max ion injection
635 time set to "Auto"); MS2 at 15,000 resolution with an AGC target of 1000% (5×10^5 ions) and a maximum injection time
636 of 22 ms, HCD fragmentation at 33% normalized collision energy, 8 *m/z* isolation window, and a loop count of 75 with an
637 inclusion list of 151 overlapping DIA windows with optimized *m/z* values generated using the tool in EncyclopeDIA. The
638 library samples were analyzed using gas-phase fractionation (28), a method wherein the same sample was injected six
639 times with each method narrowed to a 100 *m/z*-wide band of masses, i.e., 395-505, 495-605…895-1005. The DIA-MS
640 methods were the same as above except for the following: MS1 scan range was narrowed to 100 *m/z*; MS2 maximum
641 injection time of 54 ms, 4 *m/z* isolation window, and a loop count of 25 with an inclusion list of 51 overlapping DIA
642 windows.

643 *DIA data analysis:* Raw mass spectrometry data were converted to mzML using msConvert version 3.0.19106
644 (Proteowizard (88)). Peaks were centroided and the staggered DIA windows were demultiplexed (29). DIA data were
645 analyzed with EncyclopeDIA version 1.12.31 (29) using Open JDK 13 on a Slurm 19.05.5 cluster running under Ubuntu
646 20.04. Default parameters were used except the following: Percolator version 3-01 was used, Percolator training set size

647 was increased to 1M, and the -quantifyAcrossSamples flag was set to true in all cases except when exporting
648 chromatogram libraries. Spectral libraries were generated *in silico* using Prosit (27) as described previously (26). Briefly,
649 the reference *P. yoelii* 17X (89) protein FASTA database (PlasmoDB, version 55) and a mouse database (Uniref90 (90)
650 obtained from UniProt.org (91) were digested *in silico* using the tool in EncyclopeDIA (26) to obtain a list of all
651 theoretical peptides with *m/z* between 396.4 and 1004.7, two tryptic termini, up to one missed cleavage, and charge
652 state 2 or 3. This list was uploaded to Prosit (www.proteomicsdb.org/prosit/) and theoretical spectra were generated for
653 the peptides using the 2020 HCD intensity prediction model the 2019 iRT retention time prediction model, assuming an
654 NCE of 33 and a default charge state of 3. The library samples (comprising six gas-phase fractions) were searched against
655 this *in silico* library, and identified peptides were mapped to a protein database comprising the *P. yoelii* and mouse
656 protein databases and contaminants (www.thegpm.org/crap/) in order to identify degenerate peptides that could
657 theoretically come from host and contaminant proteins. The identified peptides were exported as sample-specific
658 chromatogram libraries, one for gametocytes and one for zygotes. The DIA-MS data from the biological replicates (three
659 each for gametocytes and zygotes) were searched against their respective chromatogram libraries, and separate protein
660 quantifications were carried out for the two sample types.

661 *Proteomic Data Processing:* Normalization and processing of the raw protein areas was performed in Microsoft Excel
662 (Tables S2, S3). The protein areas of the six biological replicates were log-transformed to produce normal distributions.
663 Correction factors for each sample were derived from the subset of protein areas quantified in all six samples by using z-
664 score normalization to give the subset populations the same mean and standard deviation:

665 $$x_{Corrected} = \left(\frac{(x - \mu)\sigma_{Ref}}{\sigma}\right) + \mu_{Ref}$$

666 where x is the area of a given protein in a sample, μ and σ are the average and standard deviation, respectively, of the
667 protein areas in the sample used for normalization, and *Ref* is the reference sample. After normalization, the average
668 protein area for a given protein in gametocytes or zygotes was calculated as the geometric mean, i.e., the average of the
669 log-transformed, normalized areas. Where the protein was quantified in at least two of three replicates for each sample
670 type, a p-value was calculated using a two-tailed, homoscedastic t-test. The Benjamini-Hochberg test estimated a false
671 discovery rate (FDR) of less than 8% at a p-value of 0.05. Protein abundances were considered significantly different
672 between gametocytes and zygotes if they were greater than five-fold with $p<0.05$. Additionally, in order to avoid false
673 negatives and spuriously large ratios that can arise near the limit of detection, proteins were required to be above the
674 25th percentile of abundance to be considered differently regulated.

675 To extract relative protein abundances from the gas-phase fractionated library samples, a tool in EncyclopeDIA was used
676 to combine the six gas-phase fractions for each sample type into a single data file that could be searched against the
677 Prosit *in silico* library, and a protein quantification report was generated comparing the gametocyte versus zygote library

678 samples. The reported protein area for a given protein in a given sample (gametocytes or zygotes) was only retained if
679 peptides corresponding to that protein were confidently identified (FDR < 1%) in that sample. The protein areas were
680 transformed and normalized by z-score and relative abundance percentiles were calculated as above. Absent sufficient
681 samples to perform a t-test, a p-value for each gametocyte:zygote ratio was assigned using the complementary error
682 function (erfc). The population of log-transformed gametocyte:zygote protein ratios (i.e., the difference of the log-
683 transformed and normalized protein areas) produced a normal distribution with a mean near zero, i.e., a
684 gametocyte:zygote protein abundance ratio of 1:1. A Gaussian curve with the equation:

685 $$y = Ae^{\frac{-(x-\mu)^2}{2\sigma^2}}$$

686 where A is the curve height, μ is the mean, and σ is the standard deviation, was fitted to the population using the solver
687 function in Excel. The values of μ and σ were used to calculate a p-value for each ratio x using the complementary error
688 function ERFC:

689 $$p = erfc\left(\frac{|x-\mu|}{\sqrt{2\sigma^2}}\right)$$

690 An erfc-derived p-value <0.05 corresponds to a ratio whose magnitude is greater than 95% of the ratios in the
691 population, i.e., the tails of the distribution.

692 *Searching DIA Data for Post-Translational Modifications:* Deconvoluted DIA mzML files were converted into pseudo-DDA
693 spectra using the DISCO tool in the Trans-Proteomic Pipeline (TPP) version 6.2.0 (75). The resulting spectra were
694 searched against the combined *P. yoelii*, mouse, and contaminant FASTA database using Comet version 2020.01 rev. 3
695 (92). Semi-tryptic peptides with up to two missed cleavages were allowed, with variable modifications of 15.9949 at Met
696 for oxidation, 79.966331 at Ser and Thr for phosphorylation, and 42.010565 at the protein N-terminus or the next
697 residue (in case of cleavage of N-terminal Met) for acetylation. The four experiments (biological replicate and library
698 samples of gametocytes and zygotes) were analyzed separately in the TPP using PeptideProphet and iProphet. Spectra
699 with PeptideProphet scores >0.9 and iProphet scores >0.8 were retained. Although the decoy-estimated, spectrum-level
700 FDR rate at these thresholds was <0.1%, the FDR among putatively phosphorylated spectra was ~3% owing to the fact
701 that spurious assignment of PTMs is likely to be much higher for an un-enriched sample. Only spectra with iProphet
702 scores corresponding to a decoy-estimated FDR <1% among putative phosphopeptide spectra were retained. (Table S6).

703 *Enrichment and Preparation of Gametocytes or Zygotes for TurboID Proteomics:* To generate gametocyte samples for
704 proximity proteomics, mice were injected with transgenic ALBA4::TurboID::GFP, DOZI::TurboID::GFP or the TurboID::GFP
705 control parasite line, and as the infections reached 1% parasitemia, the mice were provided with water supplemented
706 with 10 mg/L sulfadiazine (VWR, Cat# AAA12370-30) for two days. Gametocytes were selected with sulfadiazine for two

707 days before blood was collected by cardiac puncture for *ex vivo* supplementation with 150 µM biotin in RPMI 1640, 20%
708 v/v FBS at 37°C for 1 hour. After 1 hour, parasites were washed in 1x PBS three times before lysis in a modified RIPA lysis
709 buffer (50 mM Tris-HCl (pH 8.0 at room temperature), 0.1% w/v SDS, 1 mM EDTA, 150 mM NaCl, 1% v/v NP40, 0.5% w/v
710 sodium deoxycholate) with a 1x protease inhibitor cocktail (Roche, VWR, Cat# PI88266) and 0.5% v/v SUPERase In (Life
711 Technologies, Cat# AM2694) at 4°C with end-over-end rotation.

712 To generate zygote samples for proximity proteomics, mice were infected with the same TurboID transgenic parasite
713 lines as above but were not treated with sulfadiazine. When parasitemia reached 1%, blood was collected by cardiac
714 puncture into incomplete RPMI with 25mM HEPES and L-Glutamine (VWR Cat# 45000-412) at 37°C and enriched by an
715 Accudenz discontinuous gradient as described above. Briefly, the Accudenz collected cells were added to *in vitro*
716 ookinete media (RPMI 1640, 20% v/v FBS (Fisher Scientific, Cat#350-11-CV Lot # 35011126), 0.05% w/v hypoxanthine
717 (Fisher Scientific, Cat#AC122010250), 100 µM xanthurenic acid (Sigma Aldrich, Cat# D120804-1G), pH 8.2 at 22°C) and
718 were allowed to develop for 6 hours at room temperature, to allow for fertilization to occur and to enable zygote
719 development (93-95). Zygotes were observed by DIC and fluorescence microscopy (Zeiss Axioscope A1 with 8-bit
720 AxioCam ICc1 camera) using the 100X oil objective and processed by Zen 2012 (blue edition) imaging software. In the
721 final hour of zygote culture, the parasites were supplemented with 150 µM biotin to allow for biotinylation to occur.
722 After one hour, cells were washed in 1X PBS, and added to magnetic Protein G beads (Invitrogen, Cat# 10003D) coated
723 with mouse monoclonal anti-Pys25 antibody (96) to enrich for zygotes that express Pys25 on their surface away from
724 female gametocytes that do not. The enriched zygotes were lysed on-bead with the above modified RIPA lysis buffer at
725 4°C for one hour with end-over-end rotation.

726 The gametocyte and zygote lysates were mechanically lysed with a 1 mL Dounce homogenizer (Wheaton, Cat# 357538)
727 for one minute on ice with a tight pestle following chemical lysis. The parasite lysates were added to magnetic
728 Dynabeads MyOne Streptavidin T1 (Life Technologies, Cat# 65601) for three hours at 4°C with end-over-end rotation to
729 allow the streptavidin beads to bind the biotinylated proteins. The beads were washed with 'wash buffer' (50 mM Tris-
730 HCl (pH 8.0 at room temperature), 1 mM EDTA, 150 mM NaCl, 1% v/v NP40) once, and then transferred to a new tube to
731 reduce background from non-specific proteins binding to the surface of the plastic tube. The beads were washed three
732 more times with this wash buffer, then resuspended in 1x PBS. A quarter of the beads were resuspended in 2X Sample
733 Buffer (50 mM Tris-HCl (pH 6.8 at RT), 5% w/v SDS, 5% v/v glycerol, 0.16% w/v bromophenol blue, 200 mM NaCl) with a
734 fresh addition of 5% v/v β-mercaptoethanol and 1 mM biotin. Samples were then heated to 95°C to denature
735 streptavidin and elute the biotinylated proteins off the beads. The eluted proteins were removed from the beads and
736 used for affinity blot analyses, probed with anti-GFPmut2 primary antibody (1:1000 dilution, rabbit pAb, custom Pocono
737 RF&L) with anti-rabbit conjugated to HRP (1:1000 dilution, Invitrogen, Cat #A16104) or streptavidin-HRP (1:1000
738 dilution, Fisher Scientific, Novex Cat# 43-423-3) to ensure that biotinylated and bait proteins were present. Affinity blots

739 were imaged with Pierce™ ECL Western Blotting Substrate solution (Thermo Scientific, Cat# 32106) and imaged with
740 BioRad Gel Dox XR Imaging System.

741 *Tandem Mass Tag (TMT) Mass Spectrometry for the Identification of TurboID Proximal Proteins:* The on-bead captured
742 TurboID samples were analyzed by the Indiana University School of Medicine Proteomics Core. The samples were
743 digested on-bead with LysC/Trypsin in 8M urea, followed by a peptide clean-up on SPE spin columns before TMT labeling
744 with the TMTpro™ 16plex Label Reagent Set (Thermo Fisher, Cat# A44520). Peptides from each sample were labeled
745 with a distinct TMTpro™ isobaric tag before mixing. Samples were combined by sample type (e.g., unfused control
746 replicates, ALBA4 experimental replicates, DOZI experimental replicates) in equal volumes. Each mix was then run on the
747 Exploris Orbitrap mass spectrometer with 3 FAIMS (field asymmetric ion mobility spectrometry). Peptides were mapped
748 to a reference database of *P. yoelii* PY17X annotated proteins (plasmodb.org release 48) (23), *Mus musculus* proteome
749 (UniProt Proteome ID: UP000000589) (97), and the Contaminant Repository for Affinity Purification (CRAPome 2.0) using
750 Proteome Discoverer, version 2.5 to determine protein abundance values for each identified protein (98). The PY17X
751 proteins were filtered, and the average abundance values for the experimental samples and control were compared.
752 The abundance ratio was calculated to determine the enrichment of proteins detected in experimental over control
753 (abundance experimental / abundance control). A log2(abundance ratio) >2 was considered enriched in the
754 experimental sample over the control.

755 *IFA Sample Preparation and Structured Illumination Microscopy:* PyDOZI::GFP and PyNOT1-G::GFP expressing female
756 gametocytes were imaged by indirect immunofluorescence microscopy on the BioVision Technologies VT-iSIM super-
757 resolution microscope on 100X (oil) objective for high-resolution image capture of Z-slices every 1µm with MetaMorph
758 software. Images were deconvolved using the Microvolution plug-in on ImageJ, and colocalization was measured using
759 the JACoP ImageJ plug-in (72).

760 Cells were prepared for IFA as previously described (22, 40). Briefly, the transgenic gametocytes were pelleted at 1,400
761 *xg* for 3 minutes and fixed in 4% v/v paraformaldehyde (VWR, Cat# PI28908) and 0.0075% v/v glutaraldehyde (VWR,
762 Cat#AAAA17876-AE) in 1xPBS for with rocking for 30 minutes at room temperature. Cells were washed once in 1x PBS
763 and permeabilized in 1% v/v Triton X-100 (Fisher Scientific, Cat # AC327372500) for 10 minutes at room temperature.
764 Cells were well washed with 1x PBS to remove permeabilization solution before blocking with 3% w/v BSA (Sigma-
765 Aldrich, Cat # A7906-100G) in 1x PBS overnight at 4°C. Blocked cells were stained with primary antibody at 1:1000
766 dilutions in the 3% w/v BSA blocking solution for one hour at room temperature with rocking. Primary antibodies used
767 were against GFP (Mouse mAb 4C9, DSHB, Cat# DSHB-GFP-4C9), HsDDX6 (DOZI homolog, rabbit pAb) (20, 80), or
768 PyPABP1 (rabbit pAb, Pocono RF&L, custom antibody) (71). Cells were washed after incubation with the primary
769 antibody twice with 3% w/v BSA blocking solution, then resuspended in the blocking solution and incubated with the
770 secondary antibodies for 1 hour, all at 1:1000 dilutions. Secondary antibodies used were against mouse (Donkey anti-

771 mouse, AF488; Invitrogen Cat#A21202) or goat (Donkey anti-goat AF488, Invitrogen Cat# A11055) or rabbit (Donkey
772 anti-rabbit AF594, Invitrogen, Cat# A11012). Cells were washed in 1x PBS, then stained with 1 µg/mL DAPI (4',6-
773 diamidino-2-phenylindole) in 1x PBS for 5 min at room temperature. Cells were washed once in 1x PBS, then
774 resuspended in 1xPBS before mounting on glass slides in a 1:1 ratio with ProLong Gold Antifade Mountant (Invitrogen,
775 Cat# P36930), and covered with a glass cover slip before imaging.

776 *Ultrastructure Expansion Microscopy (U-ExM):* PyDOZI::GFP expressing female gametocytes were subjected to
777 ultrastructure expansion microscopy (U-ExM) as previously described (68, 99). Cells were stained with chicken anti-GFP
778 IgY fraction (Aves Labs, #GFP-1010) at a 1:1000 dilution, and counterstained with custom rabbit polyclonal antisera
779 against PyCITH, PyPABP1, or PyALBA4 (20, 70, 71) at a 1:5000 dilution. Secondary antibodies against chicken IgY
780 (Thermo, #A11039, AF488) or rabbit IgG (Thermo #A11011, AF568) were applied at a 1:500 dilution. Sytox Deep Red
781 (Thermo, #S11380, 1:1000) and NHS-Ester (Thermo, #30000, AF405, 1:250) were used to stain nucleic acids and proteins
782 as before (68, 99). Images were captured on a Zeiss LSM980 series microscope using a Plan-Apochromat 63X/1.40 Oil
783 DIC M27 objective with Airyscan 2 detector using ZEN Blue software. Z-stacks were acquired at zoom 5.0 with a 0.1 um
784 step size. Images were processed using ZEN AiryScan Joint Deconvolution Module followed by channel alignment.

785

786 **Data Availability**

787 Datasets associated with this study are publicly available: RNA-seq files are available at NCBI GEO: SRA BioProject:
788 GSE231838; GSM7304682- GSM7304686. The mass spectrometry data associated with this work are available through
789 the MassIVE repository (https://massive.ucsd.edu/) with the identifier MSV000092154 or ProteomeXchange
790 (http://www.proteomexchange.org) with the identifier PXD042955.

791 **Acknowledgments**

792 The authors would like to acknowledge the Huck Institutes' Core Facilities of Penn State at University Park that were
793 instrumental in conducting this work (Genomics: RRID:SCR_023645; Microscopy: RRID: SCR_024457). We also thank
794 Amber Mosley and Emma Doud of the Indiana University School of Medicine Proteomics Core for their expert assistance
795 in generating the tandem mass tag proteomic data, and for critical discussions of the resulting data. We are grateful to
796 Michael Tribone of the Huck Institutes for assistance in creating the model illustration (Fig 6). All of our work is greatly
797 enabled and impacted by VEuPathDB as an essential resource. We thank Takafumi Tsuboi for the provision of the anti-
798 Pys25 hybridoma. Finally, we also acknowledge members of the Llinás and Lindner laboratories for critical discussions of
799 this work.

800 **Author Contributions: (CREDIT Designations)**

801 Conceptualization: KTR, SEL
802 Data curation: KTR, AS, MF, KES, SEL
803 Formal analysis: KTR, AS, KES, SEL
804 Funding acquisition: AS, RLM, KES, SEL
805 Investigation: KTR, JPM, KES, SEL
806 Methodology: KTR, SA, MF, KES, SEL
807 Project administration: KTR, SEL
808 Resources: MF, RLM, KES, SEL
809 Software: RLM, KES
810 Supervision: SEL
811 Validation: KTR, KES
812 Visualization: KTR, JPM, KES, SEL
813 Writing – original draft: KTR, KES, SEL
814 Writing – reviewing and editing: KTR, JPM, RLM, MF, SA, KES, SEL

815 **Funding**

816 This work was supported by awards from NIAID (R01AI123341 and R56AI123341 to SEL; R01AI1484489 to KES), NIGMS
817 (R01GM087221 to RLM), the Office of the Director (S10OD026936 to RLM), the National Science Foundation (1920268
818 to RLM), and support from the Huck Institutes of the Life Sciences (AS, SEL).

819 The content is solely the responsibility of the authors and does not necessarily represent the official views of the funding
820 agencies.

821 **Financial Disclosures**

822 We have no financial disclosures associated with this study.

823 **Conflict of Interest**

824 The authors declare that they have no conflicts of interest with the contents of this article.

825 **Figure Legends**

826 **Figure 1: Comparative transcriptomics of *P. yoelii* female gametocytes and zygotes.** A. A heatmap of sample-to-sample
827 distance hierarchical clustering of biological replicates of RNA-seq data is shown. B. A Venn diagram illustrates the
828 overlapping detection of transcripts in female gametocytes and zygotes. C. Volcano plot of differentially abundant
829 transcripts enriched in female gametocytes (red) or zygotes (green). D. Dot plot of transcript abundance in female
830 gametocytes and zygotes. Differentially abundant transcripts in female gametocytes or zygotes are highlighted as red or
831 green points, respectively. E. Venn diagram of differentially abundant transcripts in zygotes and the *P. yoelii* orthologous
832 transcripts that are targets of transcription factors PbApiAP2-O and PbApiAP2-Z is shown (11, 25).

833 **Figure 2: Differential protein expression between female gametocytes and zygotes.** (A) A Venn diagram illustrates the
834 overlapping detection of proteins from the library and biological replicate samples from DIA-MS for female gametocytes
835 and zygotes. (B) A heatmap of sample-to-sample distance hierarchical clustering of biological replicates of DIA
836 proteomics is shown. (C) The total signal for each protein (measured as the sum of all quantified peptide areas for the
837 protein) from the biological replicates of samples (not the DIA-MS libraries) compared between female gametocytes and
838 zygotes is shown. The 25th abundance quartile is demarcated with dashed grey lines; only proteins detected above this
839 threshold were considered. Red circles represent proteins that are significantly differently expressed or found in only
840 one stage. Representative proteins-of-interest are labeled. More abundant/only detected in zygotes: gamete surface 6-
841 cys protein P47, ookinete surface 6-cys proteins P25 and P28, and LCCL domain-containing LAP and CCp proteins. More
842 abundant/only detected in gametocytes: gametocyte surface 6-cys proteins P230 and P48/45, perforin-like protein
843 PPLP2, and gamete egress and sporozoite traversal protein GEST.

844 **Figure 3: Identification of translationally repressed transcripts in *P. yoelii* female gametocytes that are translated**
845 **following fertilization.** A. The protein abundance ratio and RNA abundance ratio for transcripts and proteins detected in
846 female gametocytes and zygotes were compared to identify transcripts detected in female gametocytes with five-fold
847 enriched protein expression in zygotes (highlighted in black). Transcripts-of-note that are relieved from translational
848 repression are indicated in the inset box. B. Syntenic *P. yoelii* orthologs of transcripts identified in *P. falciparum* female
849 gametocytes as translationally repressed are highlighted in pink (Lasonder *et al.* (6)). C. Syntenic *P. yoelii* orthologs of
850 transcripts identified to interact with PbDOZI in *P. berghei* gametocytes are highlighted in blue (Guerreiro *et al.* (21)).

851 **Figure 4: TurboID proximity proteomics reveals changes to the major translationally repressive protein complex**
852 **across life stages.** A and B. The abundance ratios of proteins detected over control biotinylation in gametocytes and
853 zygotes for (A) PyDOZI::TurboID::GFP or (B) PyALBA4::TurboID::GFP are plotted. Abundance ratios were calculated for
854 each protein as $\frac{average\ experimental\ abundance}{average\ control\ abundance}$. Proteins with an abundance ratio > 4 were considered enriched as
855 interactions with PyDOZI or PyALBA4 over background labeling. C. Network of protein interactions-of-note detected in

856 DOZI-TurboID and ALBA4-TurboID experiments in gametocytes (left) and zygotes (right). Proteins in grey circles are
857 detected as proximal interactors of both DOZI and ALBA4, proteins in green circles are only detected as DOZI interactors,
858 and proteins in red circles are only detected as ALBA4 interactors. Colored lines represent interactions previously
859 detected in other immunoprecipitation-mass spectrometry experiments: green lines are interactions detected in PbDOZI
860 IP-MS in gametocytes from Mair *et al.* (10), red lines are interactions detected in PyALBA4 IP-MS in gametocytes from
861 Munoz *et al*. (20), and blue lines are interactions detected in PyCCR4-1 IP-MS in blood stages from Hart *et al*. (80).

862 **Figure 5: Ultrastructure expansion microscopy cross-validates protein-protein interactions in female gametocytes**.
863 PyDOZI::GFP-expressing female gametocytes were visualized via ultrastructure expansion microscopy (U-ExM) as
864 previously described (68, 99). Parasites were stained with anti-GFP to mark DOZI (yellow) and were counterstained with
865 custom rabbit polyclonal antibodies raised against PyCITH, PyPABP1, and PyALBA4 (magenta). Nucleic acids and proteins
866 were stained with Sytox Far Red (blue) and NHS-Ester (gray), respectively. Colocalization is denoted with pink coloration
867 in the merged image of a single z plane. Scale bars = 2.4 microns.

868 **Figure 6: A model of the regulation of translational repression across the host-to-vector transmission event.** (Top)
869 Proteins that can be made ahead of transmission in female gametocytes (left) or that are made shortly after fertilization
870 and formation of a zygote (right) are illustrated. (Bottom) Proximity proteomics of DOZI and ALBA4 that associate with
871 the 5' and 3' end of mRNAs, respectively, revealed conformational changes in bound mRNAs between female
872 gametocytes and zygotes, consistent with recent reports that demonstrated this by smFISH in other eukaryotes.
873 Widespread compositional changes in the DOZI/CITH/ALBA complex are also evident, especially the handoff of DOZI
874 interactions from NOT1-G to NOT1 across the transmission event.

875 **Supp Figures**

876 **Figure S1: Genomic locus and genotyping PCR for the PyApiAP2-O::GFP lines.** (Top) A genomic locus schematic of the
877 unedited wild-type locus and the transgenic locus are shown with anticipated PCR fragment sizes listed. (Bottom)
878 Genotyping PCR results for wild-type (Py17XNL), transgenic parasites (TG), no template controls (NTC), and a positive
879 plasmid control (the plasmid used to create the transgenic line) are shown.

880 **Figure S2: Flow cytometric enrichment of female gametocytes and zygotes.** A. Uninfected red blood cells were used as
881 a negative control for the collection of female gametocytes expressing green fluorescent protein (GFP) from a female-
882 enriched promoter. B. Parasites expressing GFP from the female-enriched *pylap4*$_{\text{promoter}}$ were selected by fluorescence
883 activated cell sorting and collected into RPMI kept at 37°C to prevent gametogenesis. C. Collected cells were assessed by
884 fluorescence microscopy to ensure female gametocytes were specifically enriched by FACS. D. Uninfected red blood cells
885 stained with DRAQ5 nuclear stain were used as a negative control for the collection of Pys25-positive zygotes. E. *In vitro*
886 cultured zygotes were surface stained with α-Pys25 primary antibody (mouse) and α-mouse Alexa Fluor594 secondary
887 antibody, and DRAQ5 to separate the Pys25-positive zygotes from uninfected red blood cells or other parasite life
888 stages. The cultured zygotes also expressed GFP as a fusion protein with PyApiAP2-O::GFP. F. Collected zygotes were
889 assessed by live fluorescence to ensure the expected population was enriched by FACS.

890 **Figure S3: Genomic locus and genotyping PCRs for *P. yoelii* Parasites with TurboID-GFP Fusions.** Genomic locus
891 schematics and validation data for (A) the unfused control, (B) PyALBA4, and (C) PyDOZI are provided. (Top) The
892 unedited wild-type locus and the transgenic locus are illustrated with anticipated PCR fragment sizes listed. (Bottom)
893 Genotyping PCR results for wild-type (Py17XNL), transgenic parasites (TG), no template controls (NTC), and a positive
894 plasmid control (the plasmid used to create the transgenic line) are shown.

895 **Figure S4: Quality control blots in support of TurboID experiments with female gametocytes and zygotes.** A. Schematic
896 of TurboID::GFP-tagged PyALBA4, PyDOZI, and an unfused control. Expected protein masses of each fusion protein are
897 provided. (B and C) PyALBA4 was endogenously tagged with GFP (no TurboID), BioID::GFP, or TurboID::GFP (TID). Mixed
898 blood stage parasites were supplemented without (0) or with 150uM biotin for 15 minutes (15') or 12 hours. Whole-cell
899 lysates were probed with (B) streptavidin-HRP to assess the extent of biotinylation in each sample or (C) α-GFP antibody
900 to confirm that while the efficiency of biotinylation differs between these parasite lines, the tagged proteins are present
901 at qualitatively similar abundances. (D and E) Gametocytes were similarly tested for TurboID activity in an *ex vivo* culture
902 without biotin supplementation (0) or with 150uM biotin for 15 minutes, or 1, 2, 4, or 12 hours. Unfused TID::GFP
903 gametocytes were compared with (D) PyALBA4::TID::GFP or (E) PyDOZI::TID:GFP. Whole-cell lysates were probed with
904 streptavidin-HRP to assess the extent of biotinylation in each sample. A red asterisk at the bottom of the 1-hour lane
905 indicates that this condition was selected for mass spectrometric analyses. (F) Zygotes were similarly tested for TurboID

906 activity. Zygotes were cultured *in vitro* for 6 hours, with or without supplementation with 150 µM biotin for the final
907 hour before capture on Pys25-coated magnetic Protein G beads. Unfused TID::GFP zygotes were compared with
908 PyALBA4::TID::GFP or PyDOZI::TID::GFP. Whole-cell lysates were probed with streptavidin-HRP to assess the extent of
909 biotinylation in each sample. (G and H) TurboID-based biotinylated proteins from gametocytes expressing unfused
910 TID::GFP or PyALBA4::TID::GFP were captured on streptavidin-conjugated Dynabeads. The input ("I"), flow-through ("F"),
911 and eluate ("E") were probed with (F) streptavidin-HRP or (G) α-GFP antibody as above. (I and J) The same experiment
912 but with TID::GFP and PyDOZI::TID::GFP was conducted and probed as in panels F and G. (K) TurboID-based biotinylated
913 proteins from *in vitro* zygotes expressing unfused TID::GFP, PyALBA4::TID::GFP, or PyDOZI::TID::GFP were captured on
914 streptavidin-conjugated Dynabeads. The input ("I"), flow-through ("F"), and eluate ("E") were probed with (F)
915 streptavidin-HRP.

916 **Figure S5: Comparisons to previously identified protein interactions of DOZI and ALBA4.** (A) Proteins proximal to
917 PyDOZI::TurboID::GFP and/or PyALBA4::TurboID::GFP in gametocytes were compared to the immunoprecipitated
918 PbDOZI::GFP complex in gametocytes by Mair and colleagues (10). (B) Proteins proximal to PyALBA4::TurboID::GFP in
919 gametocytes were compared to the immunoprecipitated PyALBA4::GFP complex in gametocytes by Munoz and
920 colleagues (20). (C) Proteins proximal to PyDOZI::TurboID::GFP in gametocytes were compared to the
921 immunoprecipitated PyCCR4-1::GFP complex in blood stages by Hart and colleagues (80).

922 **Figure S6: Colocalization analysis of detected protein-protein interactions in female gametocytes**. PyDOZI::GFP-
923 expressing (A) or PyNOT-1G::GFP-expressing (B) female gametocytes were used for super-resolution structured
924 illumination microscopy (3D-SIM) imaging to assess protein colocalization. The ImageJ plugin JACoP was used to assess
925 3D fluorescence colocalization for each pair of proteins indicated (72, 100). The signal intensity from the green channel
926 was compared to the corresponding pixel in the red channel for all Z-stacks of the 3D image to calculate the overlap
927 coefficient. This value varies from 0 to 1, with 0 indicating no fluorescence signal overlap and 1 reflecting complete
928 fluorescence signal colocalization.

929

930 **<u>Supp Tables</u>**

931 **Table S1: Complete datasets for RNA-seq experiments completed in this study.**

932 **Table S2: Complete datasets for DIA proteomics of spectral library samples completed in this study.**

933 **Table S3: Complete datasets for DIA proteomics of experimental samples completed in this study.**

934 **Table S4: Translationally repressed mRNAs across the host-to-vector transmission event with comparisons to previous**
935 **datasets (Guerreiro *et al*. (21), Lasonder *et al*. (6), Sebastian *et al*. (74)).**

936 **Table S5: Complete datasets of TurboID-based proximity proteomics of PyDOZI and PyALBA4 in female gametocytes**
937 **and zygotes.**

938 **Table S6: Complete dataset of post-translational modifications detected by mass spectrometry.**

939 **Table S7: Oligonucleotides used in this study. Lower case letters indicate non-homologous bases added for cloning**
940 **purposes.**

941

942 **Supp Files:**

943 **File S1: A Makefile describing the bioinformatic workflow used for RNA-seq analyses in this study.**

944 **References**

945 1. Chen H, Einstein LC, Little SC, Good MC. Spatiotemporal Patterning of Zygotic Genome Activation in a Model
946 Vertebrate Embryo. Dev Cell. 2019;49(6):852-66 e7. Epub 2019/06/19. doi: 10.1016/j.devcel.2019.05.036. PubMed
947 PMID: 31211992; PMCID: PMC6655562.
948 2. Jukam D, Shariati SAM, Skotheim JM. Zygotic Genome Activation in Vertebrates. Dev Cell. 2017;42(4):316-32.
949 Epub 2017/08/23. doi: 10.1016/j.devcel.2017.07.026. PubMed PMID: 28829942; PMCID: PMC5714289.
950 3. Lee MT, Bonneau AR, Giraldez AJ. Zygotic genome activation during the maternal-to-zygotic transition. Annu Rev
951 Cell Dev Biol. 2014;30:581-613. Epub 2014/08/26. doi: 10.1146/annurev-cellbio-100913-013027. PubMed PMID:
952 25150012; PMCID: PMC4303375.
953 4. Richter JD, Lasko P. Translational control in oocyte development. Cold Spring Harb Perspect Biol.
954 2011;3(9):a002758. Epub 2011/06/22. doi: 10.1101/cshperspect.a002758. PubMed PMID: 21690213; PMCID:
955 PMC3181033.
956 5. Hamm DC, Harrison MM. Regulatory principles governing the maternal-to-zygotic transition: insights from
957 Drosophila melanogaster. Open Biol. 2018;8(12):180183. Epub 2019/04/13. doi: 10.1098/rsob.180183. PubMed PMID:
958 30977698; PMCID: PMC6303782.
959 6. Lasonder E, Rijpma SR, van Schaijk BC, Hoeijmakers WA, Kensche PR, Gresnigt MS, Italiaander A, Vos MW,
960 Woestenenk R, Bousema T, Mair GR, Khan SM, Janse CJ, Bartfai R, Sauerwein RW. Integrated transcriptomic and
961 proteomic analyses of P. falciparum gametocytes: molecular insight into sex-specific processes and translational
962 repression. Nucleic Acids Res. 2016;44(13):6087-101. Epub 2016/06/15. doi: 10.1093/nar/gkw536. PubMed PMID:
963 27298255; PMCID: PMC5291273.
964 7. Mair GR, Braks JA, Garver LS, Wiegant JC, Hall N, Dirks RW, Khan SM, Dimopoulos G, Janse CJ, Waters AP.
965 Regulation of sexual development of Plasmodium by translational repression. Science. 2006;313(5787):667-9. Epub
966 2006/08/05. doi: 10.1126/science.1125129. PubMed PMID: 16888139; PMCID: PMC1609190.
967 8. Thompson J, Sinden RE. In situ detection of Pbs21 mRNA during sexual development of Plasmodium berghei.
968 Mol Biochem Parasitol. 1994;68(2):189-96. Epub 1994/12/01. doi: 10.1016/0166-6851(94)90164-3. PubMed PMID:
969 7739665.
970 9. Paton MG, Barker GC, Matsuoka H, Ramesar J, Janse CJ, Waters AP, Sinden RE. Structure and expression of a
971 post-transcriptionally regulated malaria gene encoding a surface protein from the sexual stages of Plasmodium berghei.
972 Mol Biochem Parasitol. 1993;59(2):263-75. Epub 1993/06/01. doi: 10.1016/0166-6851(93)90224-l. PubMed PMID:
973 8341324.
974 10. Mair GR, Lasonder E, Garver LS, Franke-Fayard BM, Carret CK, Wiegant JC, Dirks RW, Dimopoulos G, Janse CJ,
975 Waters AP. Universal features of post-transcriptional gene regulation are critical for Plasmodium zygote development.
976 PLoS Pathog. 2010;6(2):e1000767. Epub 2010/02/20. doi: 10.1371/journal.ppat.1000767. PubMed PMID: 20169188;
977 PMCID: PMC2820534.
978 11. Nishi T, Kaneko I, Iwanaga S, Yuda M. Identification of a novel AP2 transcription factor in zygotes with an
979 essential role in Plasmodium ookinete development. PLoS Pathog. 2022;18(8):e1010510. Epub 2022/08/11. doi:
980 10.1371/journal.ppat.1010510. PubMed PMID: 35947628; PMCID: PMC9394825.
981 12. Yeoh LM, Goodman CD, Mollard V, McFadden GI, Ralph SA. Comparative transcriptomics of female and male
982 gametocytes in Plasmodium berghei and the evolution of sex in alveolates. BMC Genomics. 2017;18(1):734. Epub
983 2017/09/20. doi: 10.1186/s12864-017-4100-0. PubMed PMID: 28923023; PMCID: PMC5604118.
984 13. Yuda M, Iwanaga S, Shigenobu S, Mair GR, Janse CJ, Waters AP, Kato T, Kaneko I. Identification of a transcription
985 factor in the mosquito-invasive stage of malaria parasites. Mol Microbiol. 2009;71(6):1402-14. Epub 2009/02/18. doi:
986 10.1111/j.1365-2958.2009.06609.x. PubMed PMID: 19220746.
987 14. Khan SM, Franke-Fayard B, Mair GR, Lasonder E, Janse CJ, Mann M, Waters AP. Proteome analysis of separated
988 male and female gametocytes reveals novel sex-specific Plasmodium biology. Cell. 2005;121(5):675-87. Epub
989 2005/06/07. doi: 10.1016/j.cell.2005.03.027. PubMed PMID: 15935755.
990 15. Mohammed M, Dziedziech A, Sekar V, Ernest M, Alves ESTL, Balan B, Emami SN, Biryukova I, Friedlander MR, Jex
991 A, Jacobs-Lorena M, Henriksson J, Vega-Rodriguez J, Ankarklev J. Single-Cell Transcriptomics To Define Plasmodium
992 falciparum Stage Transition in the Mosquito Midgut. Microbiol Spectr. 2023;11(2):e0367122. Epub 2023/02/28. doi:
993 10.1128/spectrum.03671-22. PubMed PMID: 36847501; PMCID: PMC10100735.

994 16. Patra KP, Johnson JR, Cantin GT, Yates JR, 3rd, Vinetz JM. Proteomic analysis of zygote and ookinete stages of
995 the avian malaria parasite Plasmodium gallinaceum delineates the homologous proteomes of the lethal human malaria
996 parasite Plasmodium falciparum. Proteomics. 2008;8(12):2492-9. Epub 2008/06/20. doi: 10.1002/pmic.200700727.
997 PubMed PMID: 18563747; PMCID: PMC2637033.
998 17. Smith RC, Barillas-Mury C. Plasmodium Oocysts: Overlooked Targets of Mosquito Immunity. Trends Parasitol.
999 2016;32(12):979-90. Epub 2016/09/19. doi: 10.1016/j.pt.2016.08.012. PubMed PMID: 27639778.
1000 18. Smith RC, Vega-Rodriguez J, Jacobs-Lorena M. The Plasmodium bottleneck: malaria parasite losses in the
1001 mosquito vector. Mem Inst Oswaldo Cruz. 2014;109(5):644-61. Epub 2014/09/04. doi: 10.1590/0074-0276130597.
1002 PubMed PMID: 25185005; PMCID: PMC4156458.
1003 19. Rios KT, Lindner SE. Protein-RNA interactions important for Plasmodium transmission. PLoS Pathog.
1004 2019;15(12):e1008095. Epub 2019/12/27. doi: 10.1371/journal.ppat.1008095. PubMed PMID: 31877193; PMCID:
1005 PMC6932754.
1006 20. Munoz EE, Hart KJ, Walker MP, Kennedy MF, Shipley MM, Lindner SE. ALBA4 modulates its stage-specific
1007 interactions and specific mRNA fates during Plasmodium yoelii growth and transmission. Mol Microbiol.
1008 2017;106(2):266-84. Epub 2017/08/09. doi: 10.1111/mmi.13762. PubMed PMID: 28787542; PMCID: PMC5688949.
1009 21. Guerreiro A, Deligianni E, Santos JM, Silva PA, Louis C, Pain A, Janse CJ, Franke-Fayard B, Carret CK, Siden-Kiamos
1010 I, Mair GR. Genome-wide RIP-Chip analysis of translational repressor-bound mRNAs in the Plasmodium gametocyte.
1011 Genome Biol. 2014;15(11):493. Epub 2014/11/25. doi: 10.1186/s13059-014-0493-0. PubMed PMID: 25418785; PMCID:
1012 PMC4234863.
1013 22. Bowman LM, Finger LE, Hart KJ, Lindner SE. Definition of constitutive and stage-enriched promoters in the
1014 rodent malaria parasite, Plasmodium yoelii. Malar J. 2020;19(1):424. Epub 2020/11/25. doi: 10.1186/s12936-020-03498-
1015 w. PubMed PMID: 33228734; PMCID: PMC7685602.
1016 23. Alvarez-Jarreta J, Amos B, Aurrecoechea C, Bah S, Barba M, Barreto A, Basenko EY, Belnap R, Blevins A, Bohme
1017 U, Brestelli J, Brown S, Callan D, Campbell LI, Christophides GK, Crouch K, Davison HR, DeBarry JD, Demko R, Doherty R,
1018 Duan Y, Dundore W, Dyer S, Falke D, Fischer S, Gajria B, Galdi D, Giraldo-Calderon GI, Harb OS, Harper E, Helb D,
1019 Howington C, Hu S, Humphrey J, Iodice J, Jones A, Judkins J, Kelly SA, Kissinger JC, Kittur N, Kwon DK, Lamoureux K, Li W,
1020 Lodha D, MacCallum RM, Maslen G, McDowell MA, Myers J, Nural MV, Roos DS, Rund SSC, Shanmugasundram A, Sitnik
1021 V, Spruill D, Starns D, Tomko SS, Wang H, Warrenfeltz S, Wieck R, Wilkinson PA, Zheng J. VEuPathDB: the eukaryotic
1022 pathogen, vector and host bioinformatics resource center in 2023. Nucleic Acids Res. 2024;52(D1):D808-D16. Epub
1023 2023/11/13. doi: 10.1093/nar/gkad1003. PubMed PMID: 37953350; PMCID: PMC10767879.
1024 24. Janse CJ, van der Klooster PF, van der Kaay HJ, van der Ploeg M, Overdulve JP. DNA synthesis in Plasmodium
1025 berghei during asexual and sexual development. Mol Biochem Parasitol. 1986;20(2):173-82. Epub 1986/08/01. doi:
1026 10.1016/0166-6851(86)90029-0. PubMed PMID: 3092048.
1027 25. Kaneko I, Iwanaga S, Kato T, Kobayashi I, Yuda M. Genome-Wide Identification of the Target Genes of AP2-O, a
1028 Plasmodium AP2-Family Transcription Factor. PLoS Pathog. 2015;11(5):e1004905. Epub 2015/05/29. doi:
1029 10.1371/journal.ppat.1004905. PubMed PMID: 26018192; PMCID: PMC4446032.
1030 26. Searle BC, Swearingen KE, Barnes CA, Schmidt T, Gessulat S, Kuster B, Wilhelm M. Generating high quality
1031 libraries for DIA MS with empirically corrected peptide predictions. Nat Commun. 2020;11(1):1548. Epub 2020/03/28.
1032 doi: 10.1038/s41467-020-15346-1. PubMed PMID: 32214105; PMCID: PMC7096433 shareholder in Proteome Software,
1033 which operates in the field of proteomics. M.W. and B.K. are founders and shareholders of OmicScouts GmbH and msAid
1034 GmbH. T.S. and S.G. are founders and shareholders of msAid GmbH. OmicScouts and msAid operate in the field of
1035 proteomics. The other authors declare no competing interests.
1036 27. Gessulat S, Schmidt T, Zolg DP, Samaras P, Schnatbaum K, Zerweck J, Knaute T, Rechenberger J, Delanghe B,
1037 Huhmer A, Reimer U, Ehrlich HC, Aiche S, Kuster B, Wilhelm M. Prosit: proteome-wide prediction of peptide tandem
1038 mass spectra by deep learning. Nat Methods. 2019;16(6):509-18. Epub 2019/05/28. doi: 10.1038/s41592-019-0426-7.
1039 PubMed PMID: 31133760.
1040 28. Pino LK, Just SC, MacCoss MJ, Searle BC. Acquiring and Analyzing Data Independent Acquisition Proteomics
1041 Experiments without Spectrum Libraries. Mol Cell Proteomics. 2020;19(7):1088-103. Epub 2020/04/22. doi:
1042 10.1074/mcp.P119.001913. PubMed PMID: 32312845; PMCID: PMC7338082.
1043 29. Searle BC, Pino LK, Egertson JD, Ting YS, Lawrence RT, MacLean BX, Villen J, MacCoss MJ. Chromatogram
1044 libraries improve peptide detection and quantification by data independent acquisition mass spectrometry. Nat

Commun. 2018;9(1):5128. Epub 2018/12/05. doi: 10.1038/s41467-018-07454-w. PubMed PMID: 30510204; PMCID: PMC6277451 Y.S.T., B.X.M. and M.J.M.) has a sponsored research agreement with Thermo Fisher Scientific, the manufacturer of the instrumentation used in this research. Additionally, M.J.M. is a paid consultant for Thermo Fisher Scientific. The remaining authors declare no competing interests.

30. Rex DAB, Patil AH, Modi PK, Kandiyil MK, Kasaragod S, Pinto SM, Tanneru N, Sijwali PS, Prasad TSK. Dissecting Plasmodium yoelii Pathobiology: Proteomic Approaches for Decoding Novel Translational and Post-Translational Modifications. ACS Omega. 2022;7(10):8246-57. Epub 2022/03/22. doi: 10.1021/acsomega.1c03892. PubMed PMID: 35309442; PMCID: PMC8928344.

31. Ecker A, Bushell ES, Tewari R, Sinden RE. Reverse genetics screen identifies six proteins important for malaria development in the mosquito. Mol Microbiol. 2008;70(1):209-20. Epub 2008/09/03. doi: 10.1111/j.1365-2958.2008.06407.x. PubMed PMID: 18761621; PMCID: PMC2658712.

32. Rao PN, Santos JM, Pain A, Templeton TJ, Mair GR. Translational repression of the cpw-wpc gene family in the malaria parasite Plasmodium. Parasitol Int. 2016;65(5 Pt A):463-71. Epub 2016/06/18. doi: 10.1016/j.parint.2016.06.007. PubMed PMID: 27312996.

33. Tsai YL, Hayward RE, Langer RC, Fidock DA, Vinetz JM. Disruption of Plasmodium falciparum chitinase markedly impairs parasite invasion of mosquito midgut. Infect Immun. 2001;69(6):4048-54. Epub 2001/05/12. doi: 10.1128/IAI.69.6.4048-4054.2001. PubMed PMID: 11349075; PMCID: PMC98468.

34. Yuda M, Yano K, Tsuboi T, Torii M, Chinzei Y. von Willebrand Factor A domain-related protein, a novel microneme protein of the malaria ookinete highly conserved throughout Plasmodium parasites. Mol Biochem Parasitol. 2001;116(1):65-72. Epub 2001/07/21. doi: 10.1016/s0166-6851(01)00304-8. PubMed PMID: 11463467.

35. Singh S, Santos JM, Orchard LM, Yamada N, van Biljon R, Painter HJ, Mahony S, Llinas M. The PfAP2-G2 transcription factor is a critical regulator of gametocyte maturation. Mol Microbiol. 2021;115(5):1005-24. Epub 2020/12/29. doi: 10.1111/mmi.14676. PubMed PMID: 33368818; PMCID: PMC8330521.

36. Tremp AZ, Sharma V, Carter V, Lasonder E, Dessens JT. LCCL protein complex formation in Plasmodium is critically dependent on LAP1. Mol Biochem Parasitol. 2017;214:87-90. Epub 2017/04/18. doi: 10.1016/j.molbiopara.2017.04.005. PubMed PMID: 28414172; PMCID: PMC5482319.

37. Pradel G, Hayton K, Aravind L, Iyer LM, Abrahamsen MS, Bonawitz A, Mejia C, Templeton TJ. A multidomain adhesion protein family expressed in Plasmodium falciparum is essential for transmission to the mosquito. J Exp Med. 2004;199(11):1533-44. Epub 2004/06/09. doi: 10.1084/jem.20031274. PubMed PMID: 15184503; PMCID: PMC2211786.

38. Guttery DS, Zeeshan M, Holder AA, Tromer EC, Tewari R. Meiosis in Plasmodium: how does it work? Trends Parasitol. 2023;39(10):812-21. Epub 2023/08/05. doi: 10.1016/j.pt.2023.07.002. PubMed PMID: 37541799.

39. Collart MA, Audebert L, Bushell M. Roles of the CCR4-Not complex in translation and dynamics of co-translation events. Wiley Interdiscip Rev RNA. 2023:e1827. Epub 2023/11/27. doi: 10.1002/wrna.1827. PubMed PMID: 38009591.

40. Hart KJ, Power BJ, Rios KT, Sebastian A, Lindner SE. The Plasmodium NOT1-G paralogue is an essential regulator of sexual stage maturation and parasite transmission. PLoS Biol. 2021;19(10):e3001434. Epub 2021/10/22. doi: 10.1371/journal.pbio.3001434. PubMed PMID: 34673764; PMCID: PMC8562791.

41. Maclean AE, Hayward JA, Huet D, van Dooren GG, Sheiner L. The mystery of massive mitochondrial complexes: the apicomplexan respiratory chain. Trends Parasitol. 2022;38(12):1041-52. Epub 2022/10/28. doi: 10.1016/j.pt.2022.09.008. PubMed PMID: 36302692; PMCID: PMC10434753.

42. Evers F, Cabrera-Orefice A, Elurbe DM, Kea-Te Lindert M, Boltryk SD, Voss TS, Huynen MA, Brandt U, Kooij TWA. Composition and stage dynamics of mitochondrial complexes in Plasmodium falciparum. Nat Commun. 2021;12(1):3820. Epub 2021/06/23. doi: 10.1038/s41467-021-23919-x. PubMed PMID: 34155201; PMCID: PMC8217502.

43. Paton DG, Childs LM, Itoe MA, Holmdahl IE, Buckee CO, Catteruccia F. Exposing Anopheles mosquitoes to antimalarials blocks Plasmodium parasite transmission. Nature. 2019;567(7747):239-43. Epub 2019/03/01. doi: 10.1038/s41586-019-0973-1. PubMed PMID: 30814727; PMCID: PMC6438179.

44. Goodman CD, Siregar JE, Mollard V, Vega-Rodriguez J, Syafruddin D, Matsuoka H, Matsuzaki M, Toyama T, Sturm A, Cozijnsen A, Jacobs-Lorena M, Kita K, Marzuki S, McFadden GI. Parasites resistant to the antimalarial atovaquone fail to transmit by mosquitoes. Science. 2016;352(6283):349-53. Epub 2016/04/16. doi: 10.1126/science.aad9279. PubMed PMID: 27081071; PMCID: PMC5149070.

45. Dessens JT, Tremp AZ, Saeed S. Crystalloids: Fascinating Parasite Organelles Essential for Malaria Transmission. Trends Parasitol. 2021;37(7):581-4. Epub 2021/05/05. doi: 10.1016/j.pt.2021.04.002. PubMed PMID: 33941493.

46. Dessens JT, Saeed S, Tremp AZ, Carter V. Malaria crystalloids: specialized structures for parasite transmission? Trends Parasitol. 2011;27(3):106-10. Epub 2011/01/18. doi: 10.1016/j.pt.2010.12.004. PubMed PMID: 21237711; PMCID: PMC3133641.
47. Qian P, Wang X, Zhong CQ, Wang J, Cai M, Nguitragool W, Li J, Cui H, Yuan J. Inner membrane complex proteomics reveals a palmitoylation regulation critical for intraerythrocytic development of malaria parasite. Elife. 2022;11. Epub 2022/07/02. doi: 10.7554/eLife.77447. PubMed PMID: 35775739; PMCID: PMC9293000.
48. Volkmann K, Pfander C, Burstroem C, Ahras M, Goulding D, Rayner JC, Frischknecht F, Billker O, Brochet M. The alveolin IMC1h is required for normal ookinete and sporozoite motility behaviour and host colonisation in Plasmodium berghei. PLoS One. 2012;7(7):e41409. Epub 2012/07/31. doi: 10.1371/journal.pone.0041409. PubMed PMID: 22844474; PMCID: PMC3402405.
49. Tremp AZ, Khater EI, Dessens JT. IMC1b is a putative membrane skeleton protein involved in cell shape, mechanical strength, motility, and infectivity of malaria ookinetes. J Biol Chem. 2008;283(41):27604-11. Epub 2008/07/25. doi: 10.1074/jbc.M801302200. PubMed PMID: 18650444; PMCID: PMC2562075.
50. Ferreira JL, Heincke D, Wichers JS, Liffner B, Wilson DW, Gilberger TW. The Dynamic Roles of the Inner Membrane Complex in the Multiple Stages of the Malaria Parasite. Front Cell Infect Microbiol. 2020;10:611801. Epub 2021/01/26. doi: 10.3389/fcimb.2020.611801. PubMed PMID: 33489940; PMCID: PMC7820811.
51. Guttery DS, Roques M, Holder AA, Tewari R. Commit and Transmit: Molecular Players in Plasmodium Sexual Development and Zygote Differentiation. Trends Parasitol. 2015;31(12):676-85. Epub 2015/10/07. doi: 10.1016/j.pt.2015.08.002. PubMed PMID: 26440790.
52. Hopp CS, Balaban AE, Bushell ES, Billker O, Rayner JC, Sinnis P. Palmitoyl transferases have critical roles in the development of mosquito and liver stages of Plasmodium. Cell Microbiol. 2016;18(11):1625-41. Epub 2016/10/26. doi: 10.1111/cmi.12601. PubMed PMID: 27084458; PMCID: PMC5565149.
53. Mlambo G, Coppens I, Kumar N. Aberrant sporogonic development of Dmc1 (a meiotic recombinase) deficient Plasmodium berghei parasites. PLoS One. 2012;7(12):e52480. Epub 2013/01/04. doi: 10.1371/journal.pone.0052480. PubMed PMID: 23285059; PMCID: PMC3528682.
54. Bennink S, Kiesow MJ, Pradel G. The development of malaria parasites in the mosquito midgut. Cell Microbiol. 2016;18(7):905-18. Epub 2016/04/26. doi: 10.1111/cmi.12604. PubMed PMID: 27111866; PMCID: PMC5089571.
55. Santos JM, Egarter S, Zuzarte-Luis V, Kumar H, Moreau CA, Kehrer J, Pinto A, Costa MD, Franke-Fayard B, Janse CJ, Frischknecht F, Mair GR. Malaria parasite LIMP protein regulates sporozoite gliding motility and infectivity in mosquito and mammalian hosts. Elife. 2017;6. Epub 2017/05/20. doi: 10.7554/eLife.24109. PubMed PMID: 28525314; PMCID: PMC5438254.
56. Tarique M, Ahmad M, Ansari A, Tuteja R. Plasmodium falciparum DOZI, an RNA helicase interacts with eIF4E. Gene. 2013;522(1):46-59. Epub 2013/04/09. doi: 10.1016/j.gene.2013.03.063. PubMed PMID: 23562722.
57. Anaguano D, Dedkhad W, Brooks CF, Cobb DW, Muralidharan V. Time-resolved proximity biotinylation implicates a porin protein in export of transmembrane malaria parasite effectors. J Cell Sci. 2023;136(20). Epub 2023/09/29. doi: 10.1242/jcs.260506. PubMed PMID: 37772444; PMCID: PMC10651097.
58. Sassmannshausen J, Bennink S, Distler U, Kuchenhoff J, Minns AM, Lindner SE, Burda PC, Tenzer S, Gilberger TW, Pradel G. Comparative proteomics of vesicles essential for the egress of Plasmodium falciparum gametocytes from red blood cells. Mol Microbiol. 2023. Epub 2023/07/26. doi: 10.1111/mmi.15125. PubMed PMID: 37492994.
59. Ambekar SV, Beck JR, Mair GR. TurboID Identification of Evolutionarily Divergent Components of the Nuclear Pore Complex in the Malaria Model Plasmodium berghei. mBio. 2022;13(5):e0181522. Epub 2022/08/31. doi: 10.1128/mbio.01815-22. PubMed PMID: 36040030; PMCID: PMC9601220.
60. Lamb IM, Rios KT, Shukla A, Ahiya AI, Morrisey J, Mell JC, Lindner SE, Mather MW, Vaidya AB. Mitochondrially targeted proximity biotinylation and proteomic analysis in Plasmodium falciparum. PLoS One. 2022;17(8):e0273357. Epub 2022/08/20. doi: 10.1371/journal.pone.0273357. PubMed PMID: 35984838; PMCID: PMC9390924.
61. Clements RL, Morano AA, Navarro FM, McGee JP, Du EW, Streva VA, Lindner SE, Dvorin JD. Identification of basal complex protein that is essential for maturation of transmission-stage malaria parasites. Proc Natl Acad Sci U S A. 2022;119(34):e2204167119. Epub 2022/08/17. doi: 10.1073/pnas.2204167119. PubMed PMID: 35972967; PMCID: PMC9407223.
62. Russell AJC, Sanderson T, Bushell E, Talman AM, Anar B, Girling G, Hunziker M, Kent RS, Martin JS, Metcalf T, Montandon R, Pandey V, Pardo M, Roberts AB, Sayers C, Schwach F, Choudhary JS, Rayner JC, Voet T, Modrzynska KK,

147 Waters AP, Lawniczak MKN, Billker O. Regulators of male and female sexual development are critical for the
148 transmission of a malaria parasite. Cell Host Microbe. 2023;31(2):305-19 e10. Epub 2023/01/13. doi:
149 10.1016/j.chom.2022.12.011. PubMed PMID: 36634679.
150 63. Mugler CF, Hondele M, Heinrich S, Sachdev R, Vallotton P, Koek AY, Chan LY, Weis K. ATPase activity of the
151 DEAD-box protein Dhh1 controls processing body formation. Elife. 2016;5. Epub 2016/11/05. doi: 10.7554/eLife.18746.
152 PubMed PMID: 27692063; PMCID: PMC5096884.
153 64. Wu T, Cheng AY, Zhang Y, Xu J, Wu J, Wen L, Li X, Liu B, Dou X, Wang P, Zhang L, Fei J, Li J, Ouyang Z, He C. KARR-
154 seq reveals cellular higher-order RNA structures and RNA-RNA interactions. Nat Biotechnol. 2024. Epub 2024/01/19. doi:
155 10.1038/s41587-023-02109-8. PubMed PMID: 38238480.
156 65. Metkar M, Ozadam H, Lajoie BR, Imakaev M, Mirny LA, Dekker J, Moore MJ. Higher-Order Organization
157 Principles of Pre-translational mRNPs. Mol Cell. 2018;72(4):715-26 e3. Epub 2018/11/13. doi:
158 10.1016/j.molcel.2018.09.012. PubMed PMID: 30415953; PMCID: PMC6239896.
159 66. Adivarahan S, Livingston N, Nicholson B, Rahman S, Wu B, Rissland OS, Zenklusen D. Spatial Organization of
160 Single mRNPs at Different Stages of the Gene Expression Pathway. Mol Cell. 2018;72(4):727-38 e5. Epub 2018/11/13.
161 doi: 10.1016/j.molcel.2018.10.010. PubMed PMID: 30415950; PMCID: PMC6592633.
162 67. Khong A, Parker R. mRNP architecture in translating and stress conditions reveals an ordered pathway of mRNP
163 compaction. J Cell Biol. 2018;217(12):4124-40. Epub 2018/10/17. doi: 10.1083/jcb.201806183. PubMed PMID:
164 30322972; PMCID: PMC6279387.
165 68. Liffner B, Absalon S. Expansion Microscopy Reveals Plasmodium falciparum Blood-Stage Parasites Undergo
166 Anaphase with A Chromatin Bridge in the Absence of Mini-Chromosome Maintenance Complex Binding Protein.
167 Microorganisms. 2021;9(11). Epub 2021/11/28. doi: 10.3390/microorganisms9112306. PubMed PMID: 34835432;
168 PMCID: PMC8620465.
169 69. Bertiaux E, Balestra AC, Bournonville L, Louvel V, Maco B, Soldati-Favre D, Brochet M, Guichard P, Hamel V.
170 Expansion microscopy provides new insights into the cytoskeleton of malaria parasites including the conservation of a
171 conoid. PLoS Biol. 2021;19(3):e3001020. Epub 2021/03/12. doi: 10.1371/journal.pbio.3001020. PubMed PMID:
172 33705377; PMCID: PMC7951857.
173 70. Bennink S, von Bohl A, Ngwa CJ, Henschel L, Kuehn A, Pilch N, Weissbach T, Rosinski AN, Scheuermayer M,
174 Repnik U, Przyborski JM, Minns AM, Orchard LM, Griffiths G, Lindner SE, Llinas M, Pradel G. A seven-helix protein
175 constitutes stress granules crucial for regulating translation during human-to-mosquito transmission of Plasmodium
176 falciparum. PLoS Pathog. 2018;14(8):e1007249. Epub 2018/08/23. doi: 10.1371/journal.ppat.1007249. PubMed PMID:
177 30133543; PMCID: PMC6122839.
178 71. Minns AM, Hart KJ, Subramanian S, Hafenstein S, Lindner SE. Nuclear, Cytosolic, and Surface-Localized Poly(A)-
179 Binding Proteins of Plasmodium yoelii. mSphere. 2018;3(1). Epub 2018/01/24. doi: 10.1128/mSphere.00435-17. PubMed
180 PMID: 29359180; PMCID: PMC5760745.
181 72. Bolte S, Cordelieres FP. A guided tour into subcellular colocalization analysis in light microscopy. J Microsc.
182 2006;224(Pt 3):213-32. Epub 2007/01/11. doi: 10.1111/j.1365-2818.2006.01706.x. PubMed PMID: 17210054.
183 73. Ong HW, Adderley J, Tobin AB, Drewry DH, Doerig C. Parasite and host kinases as targets for antimalarials.
184 Expert Opin Ther Targets. 2023;27(2):151-69. Epub 2023/03/22. doi: 10.1080/14728222.2023.2185511. PubMed PMID:
185 36942408.
186 74. Sebastian S, Brochet M, Collins MO, Schwach F, Jones ML, Goulding D, Rayner JC, Choudhary JS, Billker O. A
187 Plasmodium calcium-dependent protein kinase controls zygote development and transmission by translationally
188 activating repressed mRNAs. Cell Host Microbe. 2012;12(1):9-19. Epub 2012/07/24. doi: 10.1016/j.chom.2012.05.014.
189 PubMed PMID: 22817984; PMCID: PMC3414820.
190 75. Deutsch EW, Mendoza L, Shteynberg DD, Hoopmann MR, Sun Z, Eng JK, Moritz RL. Trans-Proteomic Pipeline:
191 Robust Mass Spectrometry-Based Proteomics Data Analysis Suite. J Proteome Res. 2023;22(2):615-24. Epub 2023/01/18.
192 doi: 10.1021/acs.jproteome.2c00624. PubMed PMID: 36648445; PMCID: PMC10166710.
193 76. Lotthammer JM, Ginell GM, Griffith D, Emenecker RJ, Holehouse AS. Direct prediction of intrinsically disordered
194 protein conformational properties from sequences. Nature Methods. 2024. doi: 10.1038/s41592-023-02159-5.
195 77. Lindner SE, Swearingen KE, Shears MJ, Walker MP, Vrana EN, Hart KJ, Minns AM, Sinnis P, Moritz RL, Kappe SHI.
196 Transcriptomics and proteomics reveal two waves of translational repression during the maturation of malaria parasite

197 sporozoites. Nat Commun. 2019;10(1):4964. Epub 2019/11/02. doi: 10.1038/s41467-019-12936-6. PubMed PMID:
198 31673027; PMCID: PMC6823429.
199 78. Linder P, Jankowsky E. From unwinding to clamping - the DEAD box RNA helicase family. Nat Rev Mol Cell Biol.
200 2011;12(8):505-16. Epub 2011/07/23. doi: 10.1038/nrm3154. PubMed PMID: 21779027.
201 79. Jongco AM, Ting LM, Thathy V, Mota MM, Kim K. Improved transfection and new selectable markers for the
202 rodent malaria parasite Plasmodium yoelii. Mol Biochem Parasitol. 2006;146(2):242-50. Epub 2006/02/07. doi:
203 10.1016/j.molbiopara.2006.01.001. PubMed PMID: 16458371.
204 80. Hart KJ, Oberstaller J, Walker MP, Minns AM, Kennedy MF, Padykula I, Adams JH, Lindner SE. Plasmodium male
205 gametocyte development and transmission are critically regulated by the two putative deadenylases of the
206 CAF1/CCR4/NOT complex. PLoS Pathog. 2019;15(1):e1007164. Epub 2019/02/01. doi: 10.1371/journal.ppat.1007164.
207 PubMed PMID: 30703164; PMCID: PMC6355032.
208 81. Lindner SE, Mikolajczak SA, Vaughan AM, Moon W, Joyce BR, Sullivan WJ, Jr., Kappe SH. Perturbations of
209 Plasmodium Puf2 expression and RNA-seq of Puf2-deficient sporozoites reveal a critical role in maintaining RNA
210 homeostasis and parasite transmissibility. Cell Microbiol. 2013;15(7):1266-83. Epub 2013/01/30. doi:
211 10.1111/cmi.12116. PubMed PMID: 23356439; PMCID: PMC3815636.
212 82. Mikolajczak SA, Aly AS, Dumpit RF, Vaughan AM, Kappe SH. An efficient strategy for gene targeting and
213 phenotypic assessment in the Plasmodium yoelii rodent malaria model. Mol Biochem Parasitol. 2008;158(2):213-6. Epub
214 2008/02/05. doi: 10.1016/j.molbiopara.2007.12.006. PubMed PMID: 18242728.
215 83. Kim D, Langmead B, Salzberg SL. HISAT: a fast spliced aligner with low memory requirements. Nat Methods.
216 2015;12(4):357-60. Epub 2015/03/10. doi: 10.1038/nmeth.3317. PubMed PMID: 25751142; PMCID: PMC4655817.
217 84. Liao Y, Smyth GK, Shi W. featureCounts: an efficient general purpose program for assigning sequence reads to
218 genomic features. Bioinformatics. 2014;30(7):923-30. Epub 2013/11/15. doi: 10.1093/bioinformatics/btt656. PubMed
219 PMID: 24227677.
220 85. Love MI, Huber W, Anders S. Moderated estimation of fold change and dispersion for RNA-seq data with
221 DESeq2. Genome Biol. 2014;15(12):550. Epub 2014/12/18. doi: 10.1186/s13059-014-0550-8. PubMed PMID: 25516281;
222 PMCID: PMC4302049.
223 86. Wang L, Nie J, Sicotte H, Li Y, Eckel-Passow JE, Dasari S, Vedell PT, Barman P, Wang L, Weinshiboum R, Jen J,
224 Huang H, Kohli M, Kocher JP. Measure transcript integrity using RNA-seq data. BMC Bioinformatics. 2016;17:58. Epub
225 2016/02/05. doi: 10.1186/s12859-016-0922-z. PubMed PMID: 26842848; PMCID: PMC4739097.
226 87. Ludwig KR, Schroll MM, Hummon AB. Comparison of In-Solution, FASP, and S-Trap Based Digestion Methods for
227 Bottom-Up Proteomic Studies. J Proteome Res. 2018;17(7):2480-90. Epub 2018/05/15. doi:
228 10.1021/acs.jproteome.8b00235. PubMed PMID: 29754492; PMCID: PMC9319029.
229 88. Chambers MC, Maclean B, Burke R, Amodei D, Ruderman DL, Neumann S, Gatto L, Fischer B, Pratt B, Egertson J,
230 Hoff K, Kessner D, Tasman N, Shulman N, Frewen B, Baker TA, Brusniak MY, Paulse C, Creasy D, Flashner L, Kani K,
231 Moulding C, Seymour SL, Nuwaysir LM, Lefebvre B, Kuhlmann F, Roark J, Rainer P, Detlev S, Hemenway T, Huhmer A,
232 Langridge J, Connolly B, Chadick T, Holly K, Eckels J, Deutsch EW, Moritz RL, Katz JE, Agus DB, MacCoss M, Tabb DL,
233 Mallick P. A cross-platform toolkit for mass spectrometry and proteomics. Nat Biotechnol. 2012;30(10):918-20. Epub
234 2012/10/12. doi: 10.1038/nbt.2377. PubMed PMID: 23051804; PMCID: PMC3471674.
235 89. Otto TD, Bohme U, Jackson AP, Hunt M, Franke-Fayard B, Hoeijmakers WA, Religa AA, Robertson L, Sanders M,
236 Ogun SA, Cunningham D, Erhart A, Billker O, Khan SM, Stunnenberg HG, Langhorne J, Holder AA, Waters AP, Newbold CI,
237 Pain A, Berriman M, Janse CJ. A comprehensive evaluation of rodent malaria parasite genomes and gene expression.
238 BMC Biol. 2014;12:86. Epub 2014/11/02. doi: 10.1186/s12915-014-0086-0. PubMed PMID: 25359557; PMCID:
239 PMC4242472.
240 90. Suzek BE, Wang Y, Huang H, McGarvey PB, Wu CH, UniProt C. UniRef clusters: a comprehensive and scalable
241 alternative for improving sequence similarity searches. Bioinformatics. 2015;31(6):926-32. Epub 2014/11/16. doi:
242 10.1093/bioinformatics/btu739. PubMed PMID: 25398609; PMCID: PMC4375400.
243 91. UniProt C. UniProt: the universal protein knowledgebase in 2021. Nucleic Acids Res. 2021;49(D1):D480-D9. Epub
244 2020/11/26. doi: 10.1093/nar/gkaa1100. PubMed PMID: 33237286; PMCID: PMC7778908.
245 92. Eng JK, Hoopmann MR, Jahan TA, Egertson JD, Noble WS, MacCoss MJ. A deeper look into Comet--
246 implementation and features. J Am Soc Mass Spectrom. 2015;26(11):1865-74. Epub 2015/06/28. doi: 10.1007/s13361-
247 015-1179-x. PubMed PMID: 26115965; PMCID: PMC4607604.

248 93. Rios KT, Dickson TM, Lindner SE. Standard Selection Treatments with Sulfadiazine Limit Plasmodium yoelii Host-
249 to-Vector Transmission. mSphere. 2022;7(3):e0010622. Epub 2022/05/20. doi: 10.1128/msphere.00106-22. PubMed
250 PMID: 35586987; PMCID: PMC9241536.
251 94. Modrzynska K, Pfander C, Chappell L, Yu L, Suarez C, Dundas K, Gomes AR, Goulding D, Rayner JC, Choudhary J,
252 Billker O. A Knockout Screen of ApiAP2 Genes Reveals Networks of Interacting Transcriptional Regulators Controlling the
253 Plasmodium Life Cycle. Cell Host Microbe. 2017;21(1):11-22. Epub 2017/01/13. doi: 10.1016/j.chom.2016.12.003.
254 PubMed PMID: 28081440; PMCID: PMC5241200.
255 95. Janse CJ, Mons B, Rouwenhorst RJ, Van der Klooster PF, Overdulve JP, Van der Kaay HJ. In vitro formation of
256 ookinetes and functional maturity of Plasmodium berghei gametocytes. Parasitology. 1985;91 (Pt 1):19-29. Epub
257 1985/08/01. doi: 10.1017/s0031182000056481. PubMed PMID: 2863802.
258 96. Tsuboi T, Cao YM, Hitsumoto Y, Yanagi T, Kanbara H, Torii M. Two antigens on zygotes and ookinetes of
259 Plasmodium yoelii and Plasmodium berghei that are distinct targets of transmission-blocking immunity. Infect Immun.
260 1997;65(6):2260-4. Epub 1997/06/01. doi: 10.1128/iai.65.6.2260-2264.1997. PubMed PMID: 9169761; PMCID:
261 PMC175313.
262 97. Church DM, Goodstadt L, Hillier LW, Zody MC, Goldstein S, She X, Bult CJ, Agarwala R, Cherry JL, DiCuccio M,
263 Hlavina W, Kapustin Y, Meric P, Maglott D, Birtle Z, Marques AC, Graves T, Zhou S, Teague B, Potamousis K, Churas C,
264 Place M, Herschleb J, Runnheim R, Forrest D, Amos-Landgraf J, Schwartz DC, Cheng Z, Lindblad-Toh K, Eichler EE, Ponting
265 CP, Mouse Genome Sequencing C. Lineage-specific biology revealed by a finished genome assembly of the mouse. PLoS
266 Biol. 2009;7(5):e1000112. Epub 2009/05/27. doi: 10.1371/journal.pbio.1000112. PubMed PMID: 19468303; PMCID:
267 PMC2680341.
268 98. Mellacheruvu D, Wright Z, Couzens AL, Lambert JP, St-Denis NA, Li T, Miteva YV, Hauri S, Sardiu ME, Low TY,
269 Halim VA, Bagshaw RD, Hubner NC, Al-Hakim A, Bouchard A, Faubert D, Fermin D, Dunham WH, Goudreault M, Lin ZY,
270 Badillo BG, Pawson T, Durocher D, Coulombe B, Aebersold R, Superti-Furga G, Colinge J, Heck AJ, Choi H, Gstaiger M,
271 Mohammed S, Cristea IM, Bennett KL, Washburn MP, Raught B, Ewing RM, Gingras AC, Nesvizhskii AI. The CRAPome: a
272 contaminant repository for affinity purification-mass spectrometry data. Nat Methods. 2013;10(8):730-6. Epub
273 2013/08/08. doi: 10.1038/nmeth.2557. PubMed PMID: 23921808; PMCID: PMC3773500.
274 99. Liffner B, Cepeda Diaz AK, Blauwkamp J, Anaguano D, Frolich S, Muralidharan V, Wilson DW, Dvorin J, Absalon S.
275 Atlas of Plasmodium falciparum intraerythrocytic development using expansion microscopy. bioRxiv. 2023. Epub
276 2023/03/31. doi: 10.1101/2023.03.22.533773. PubMed PMID: 36993606; PMCID: PMC10055389.
277 100. Schindelin J, Arganda-Carreras I, Frise E, Kaynig V, Longair M, Pietzsch T, Preibisch S, Rueden C, Saalfeld S,
278 Schmid B, Tinevez JY, White DJ, Hartenstein V, Eliceiri K, Tomancak P, Cardona A. Fiji: an open-source platform for
279 biological-image analysis. Nat Methods. 2012;9(7):676-82. Epub 2012/06/30. doi: 10.1038/nmeth.2019. PubMed PMID:
280 22743772; PMCID: PMC3855844.

281

Rios *et al.* (2024) Figure 1

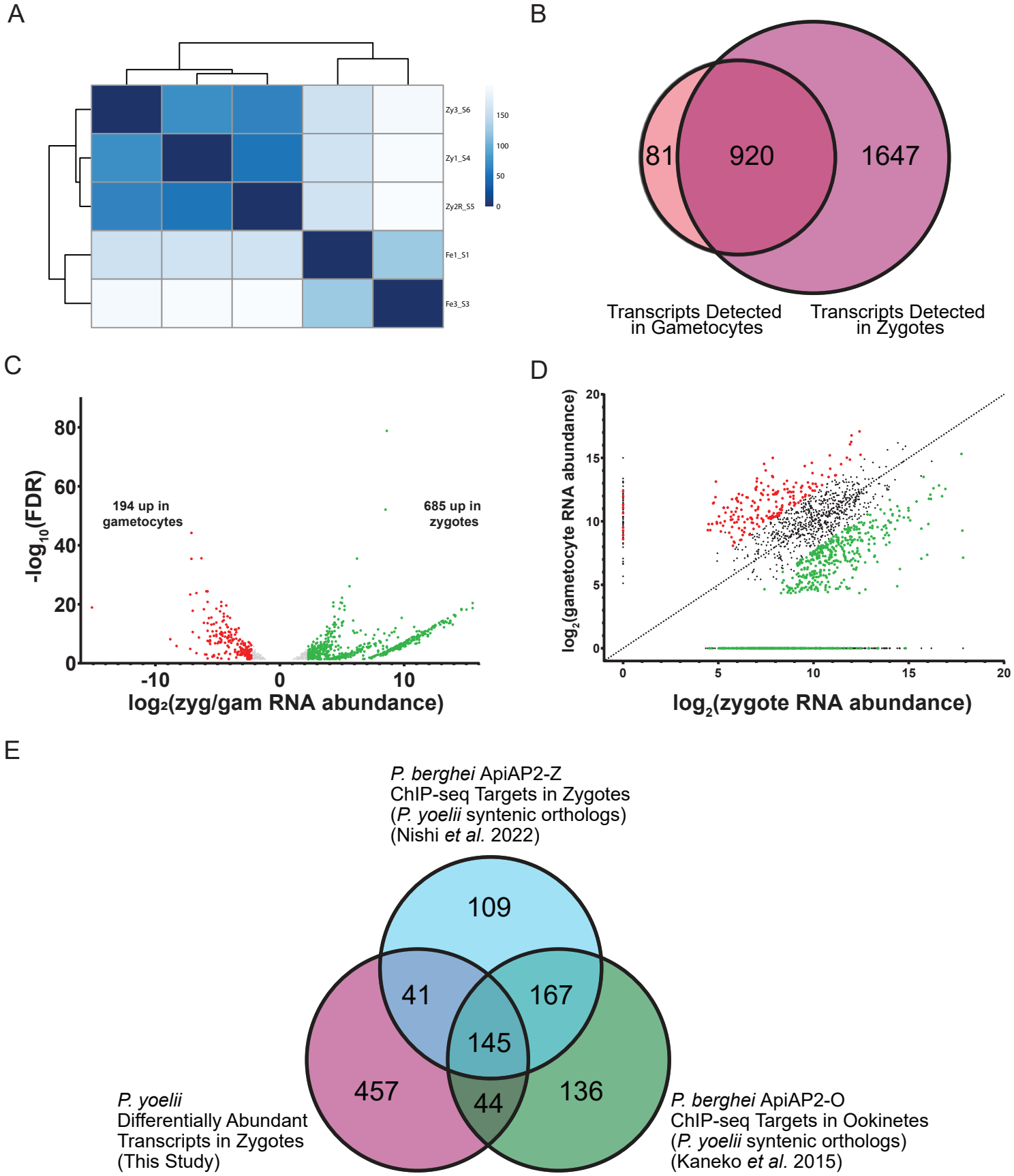

Figure 1: Comparative transcriptomics of *P. yoelii* female gametocytes and zygotes. A. A heatmap of sample-to-sample distance hierarchical clustering of biological replicates of RNA-seq data is shown. B. A Venn diagram illustrates the overlapping detection of transcripts in female gametocytes and zygotes. C. Volcano plot of differentially abundant transcripts enriched in female gametocytes (red) or zygotes (green). D. Dot plot of transcript abundance in female gametocytes and zygotes. Differentially abundant transcripts in female gametocytes or zygotes are highlighted as red or green points, respectively. E. Venn diagram of differentially abundant transcripts in zygotes and the *P. yoelii* orthologous transcripts that are targets of transcription factors PbApiAP2-O and PbApiAP2-Z is shown (11, 25).

Rios *et al.* (2024) Figure 2

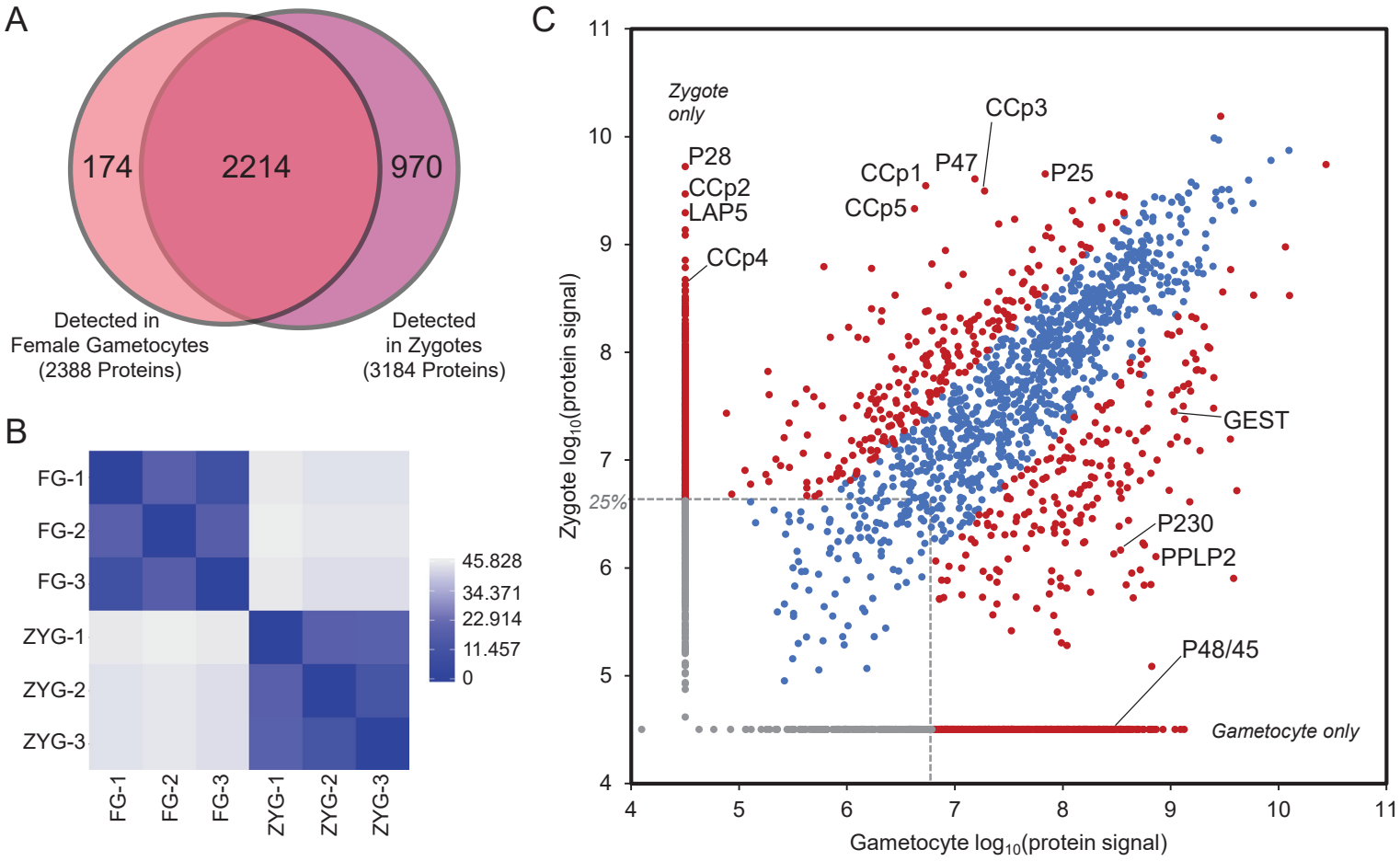

Figure 2: Differential protein expression between female gametocytes and zygotes. (A) A Venn diagram illustrates the overlapping detection of proteins from the library and biological replicate samples from DIA-MS for female gametocytes and zygotes. (B) A heatmap of sample-to-sample distance hierarchical clustering of biological replicates of DIA proteomics is shown. (C) The total signal for each protein (measured as the sum of all quantified peptide areas for the protein) from the biological replicates of samples (not the DIA-MS libraries) compared between female gametocytes and zygotes is shown. The 25th abundance quartile is demarcated with dashed grey lines; only proteins detected above this threshold were considered. Red circles represent proteins that are significantly differently expressed or found in only one stage. Representative proteins-of-interest are labeled. More abundant/only detected in zygotes: gamete surface 6-cys protein P47, ookinete surface 6-cys proteins P25 and P28, and LCCL domain-containing LAP and CCp proteins. More abundant/only detected in gametocytes: gametocyte surface 6-cys proteins P230 and P48/45, perforin-like protein PPLP2, and gamete egress and sporozoite traversal protein GEST.

Rios *et al.* (2024) Figure 3

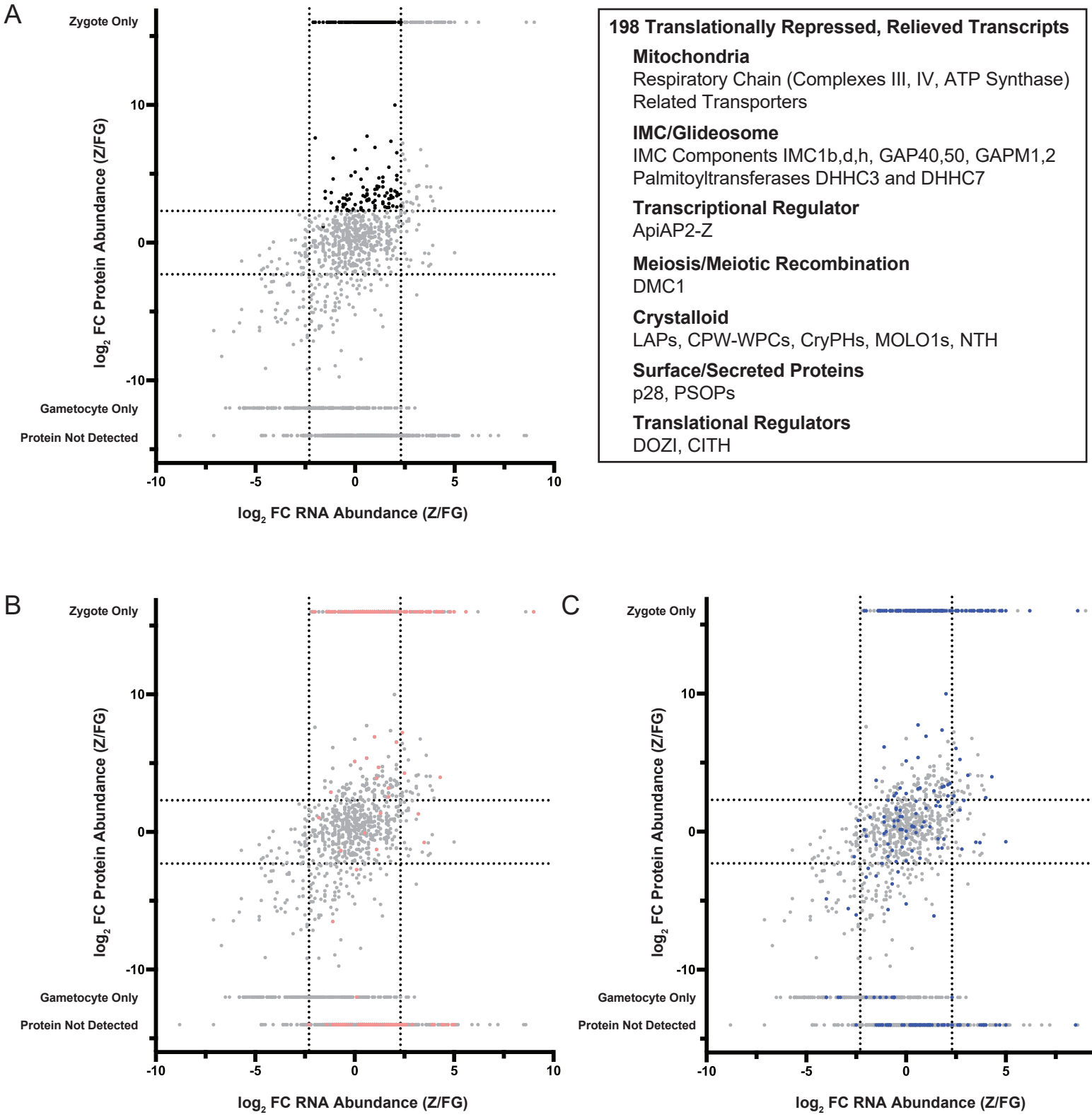

Figure 3: Identification of translationally repressed transcripts in *P. yoelii* female gametocytes that are translated following fertilization. A. The protein abundance ratio and RNA abundance ratio for transcripts and proteins detected in female gametocytes and zygotes were compared to identify transcripts detected in female gametocytes with five-fold enriched protein expression in zygotes (highlighted in black). Transcripts-of-note that are relieved from translational repression are indicated in the inset box. B. Syntenic *P. yoelii* orthologs of transcripts identified in *P. falciparum* female gametocytes as translationally repressed are highlighted in pink (Lasonder *et al*. (6)). C. Syntenic *P. yoelii* orthologs of transcripts identified to interact with PbDOZI in *P. berghei* gametocytes are highlighted in blue (Guerreiro *et al*. (21)).

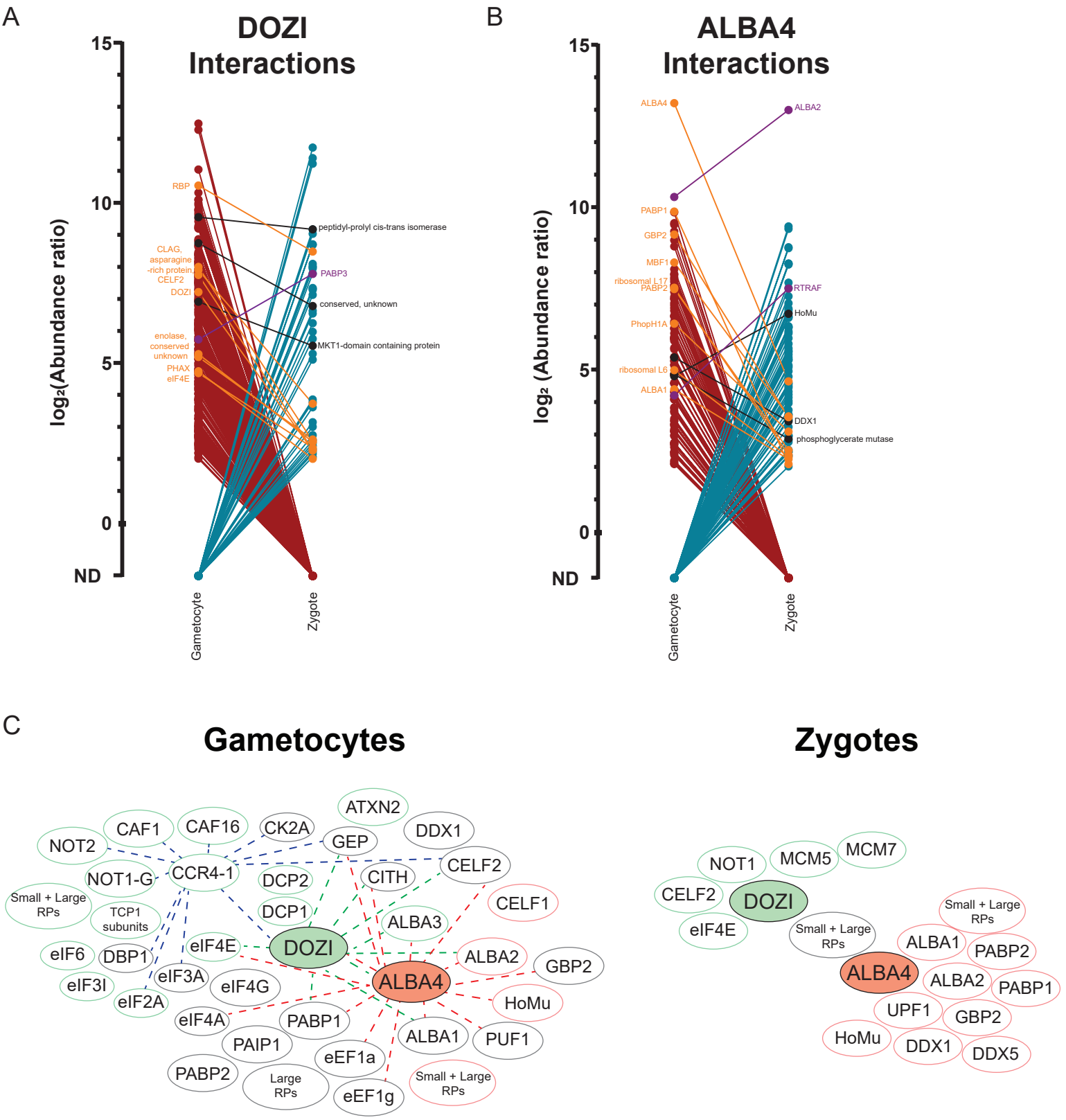

Figure 4: TurboID proximity proteomics reveals changes to the major translationally repressive protein complex across life stages. A and B. The abundance ratios of proteins detected over control biotinylation in gametocytes and zygotes for (A) PyDOZI::TurboID::GFP or (B) PyALBA4::TurboID::GFP are plotted. Abundance ratios were calculated for each protein as (average experimental abundance)/(average control abundance). Proteins with an abundance ratio > 4 were considered enriched as interactions with PyDOZI or PyALBA4 over background labeling. C. Network of protein interactions-of-note detected in DOZI-TurboID and ALBA4-TurboID experiments in gametocytes (left) and zygotes (right). Proteins in grey circles are detected as proximal interactors of both DOZI and ALBA4, proteins in green circles are only detected as DOZI interactors, and proteins in red circles are only detected as ALBA4 interactors. Colored lines represent interactions previously detected in other immunoprecipitation-mass spectrometry experiments: green lines are interactions detected in PbDOZI IP-MS in gametocytes from Mair *et al*. (10), red lines are interactions detected in PyALBA4 IP-MS in gametocytes from Munoz *et al*. (20), and blue lines are interactions detected in PyCCR4-1 IP-MS in blood stages from Hart *et al*. (79).

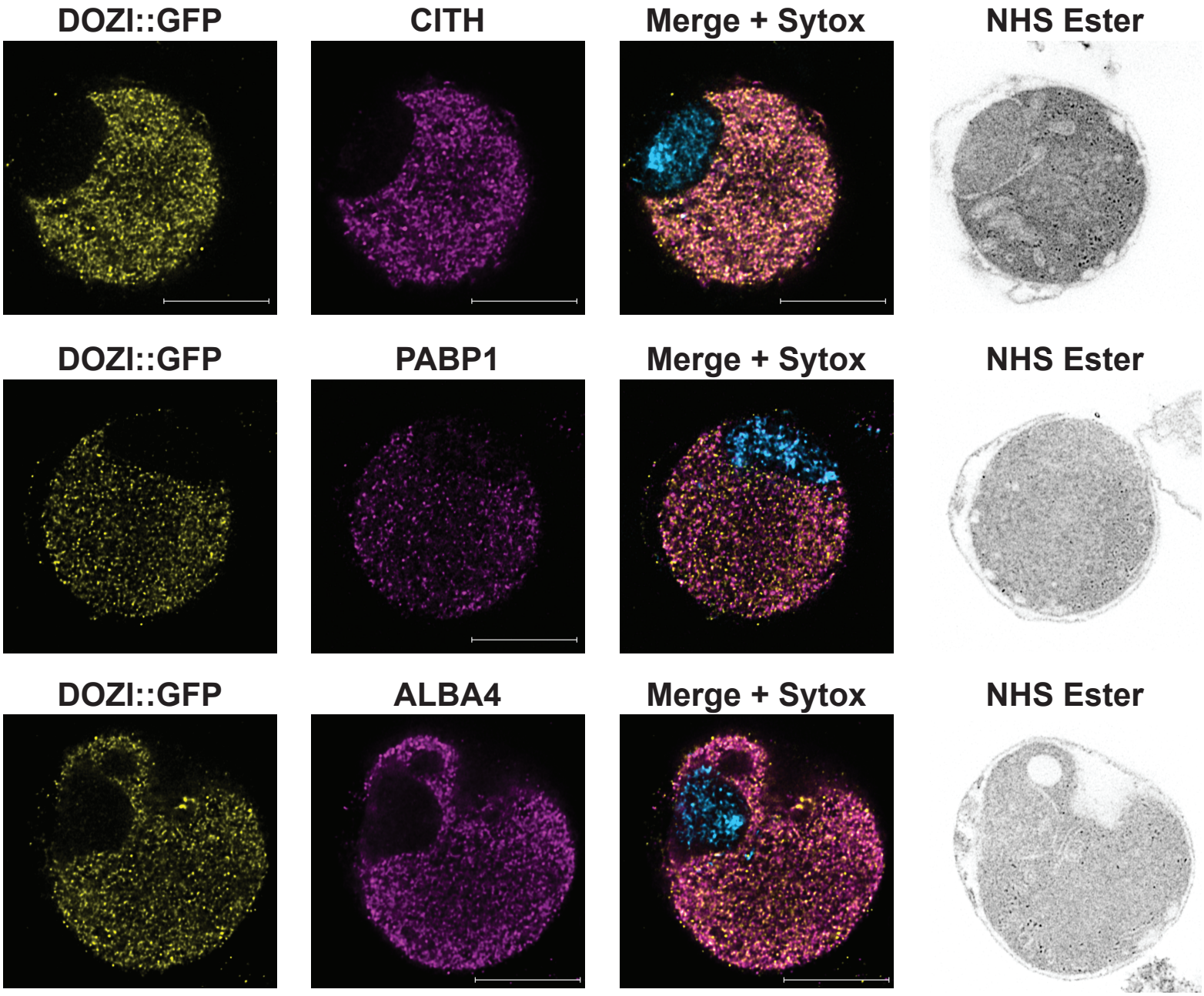

Figure 5: Ultrastructure expansion microscopy cross-validates protein-protein interactions in female gametocytes. PyDOZI::GFP-expressing female gametocytes were visualized via ultrastructure expansion microscopy (U-ExM) as previously described (67, 98). Parasites were stained with anti-GFP to mark DOZI (yellow) and were counterstained with custom rabbit polyclonal antibodies raised against PyCITH, PyPABP1, and PyALBA4 (magenta). Nucleic acids and proteins were stained with Sytox Far Red (blue) and NHS-Ester (gray), respectively. Colocalization is denoted with pink coloration in the merged image of a single z plane. Scale bars = 2.4 microns.

Rios *et al.* (2024) Figure 6

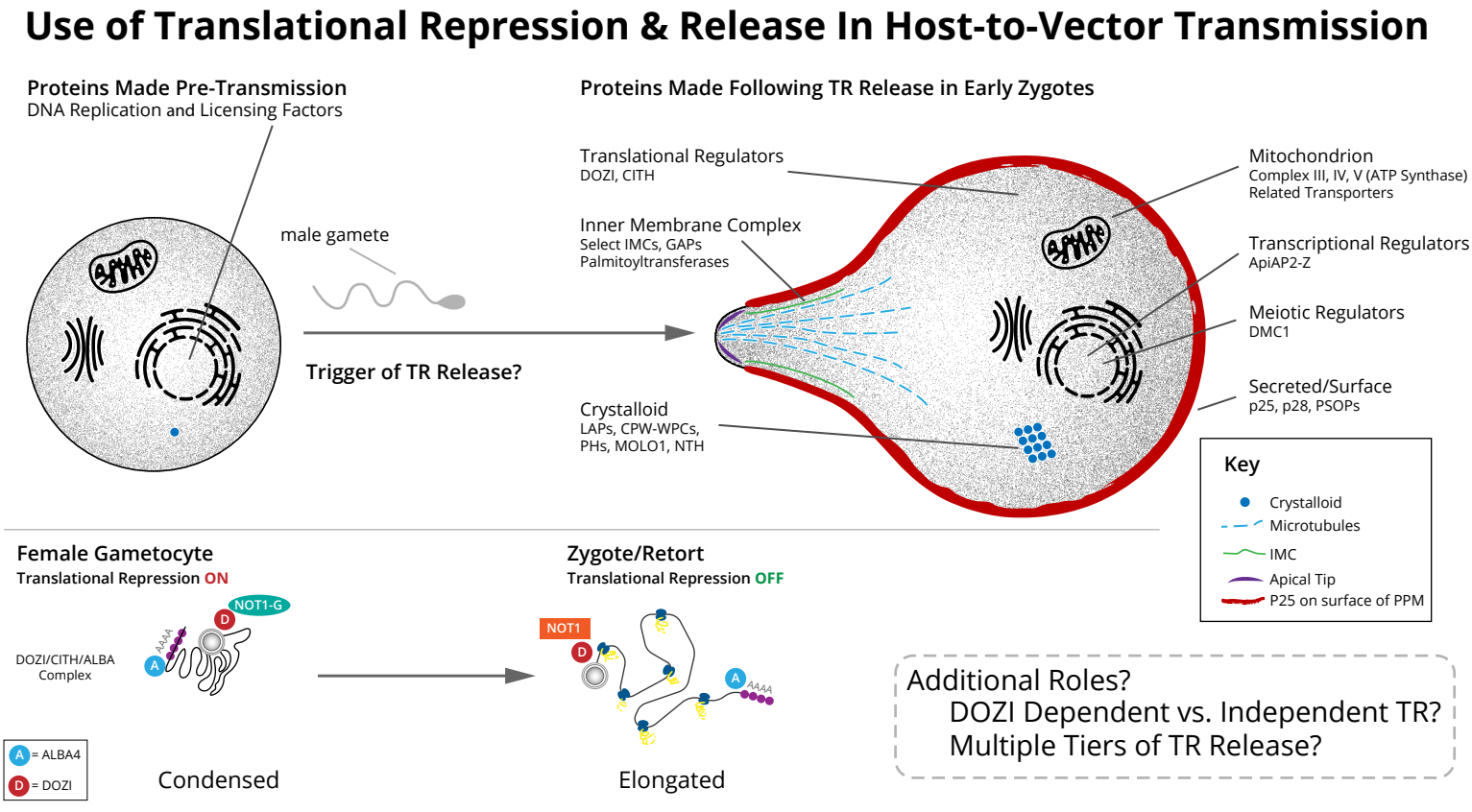

Figure 6: A model of the regulation of translational repression across the host-to-vector transmission event. (Top) Proteins that can be made ahead of transmission in female gametocytes (left) or that are made shortly after fertilization and formation of a zygote (right) are illustrated. (Bottom) Proximity proteomics of DOZI and ALBA4 that associate with the 5' and 3' end of mRNAs, respectively, revealed conformational changes in bound mRNAs between female gametocytes and zygotes, consistent with recent reports that demonstrated this by smFISH in other eukaryotes. Widespread compositional changes in the DOZI/CITH/ALBA complex are also evident, especially the handoff of DOZI interactions from NOT1-G to NOT1 across the transmission event.